AD 653891

NRL Memorandum Report 1815

Preparation and Characterization of Ultra-Pure Solids

Annual Report
July 1, 1966 - June 30, 1967
on
ARPA Order 418

C. C. Klick, G. T. Rado, M. R. Achter, and A. I. Schindler

1967

DDC
RECEIVED
JAN 18 1968
C

CLEARINGHOUSE

NAVAL RESEARCH LABORATORY
Washington, D.C.

This document has been approved for public release and sale; its distribution is unlimited.

19

DISCLAIMER NOTICE

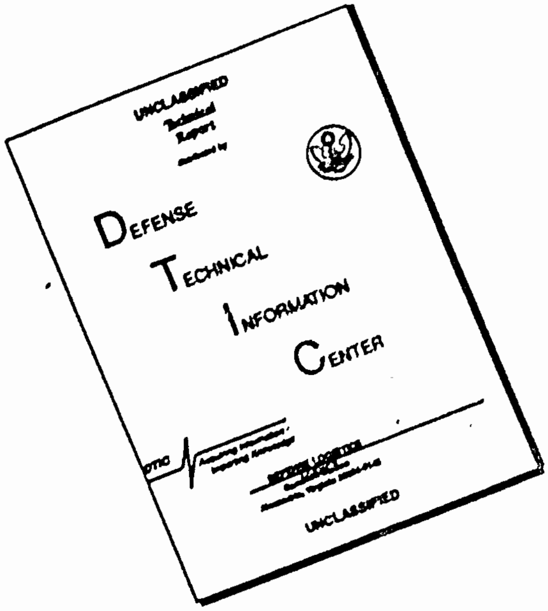

THIS DOCUMENT IS BEST QUALITY AVAILABLE. THE COPY FURNISHED TO DTIC CONTAINED A SIGNIFICANT NUMBER OF PAGES WHICH DO NOT REPRODUCE LEGIBLY.

CONTENTS

PREFACE

The Naval Research Laboratory is conducting a broad investigation on the preparation and characteristics of ultrapure imperfection-free solids in an effort to improve our understanding of the relationships between the behavior of materials and their fundamental physicochemical make-up.

Specific efforts during 1966-1967, as was the case in previous annual reports for 1964-1965 and 1965-1966, included a wide range of theoretical and experimental studies on crystal growth kinetics, metallic behavior, the nature of interactions responsible for the magnetic properties of spin-ordered materials, and optical and radiation-sensitive properties of non-metallic materials. The properties investigated were correspondingly wide, as were the types of materials chosen for study which included refractory and transition metals and alloys, intermetallic compounds, alkali halides, glasses, and certain spin-ordered substances.

Four areas of investigation showing considerable progress during the year starting July 1966 are discussed herein. These investigations, each under the cognizance of a separate research group at the Laboratory, cover accomplishments on glasses and alkali halide crystals, refractory metal crystals, transition metal crystals, and magnetic materials.

During the first portion of the past year the program on preparat of ultrapure alkali halide crystals continued the further development of methods of purification of raw materials, methods of crystal growth, and characterization of the final products. Several projects within the Optical Materials Branch were appreciably aided by the resources developed in this program. Several months after the beginning of the report year a proposal was made to enlarge in a very substantial way the effort going on in glasses and to emphasize the research aspects concerned with understanding the most fundamental properties of glass. Approval of the plan came near the beginning of the present calendar year. The character of the work changed dramatically during the last portion of the year from concentration on alkali halides to major effort on glasses. Three new members were added to the staff of the Optical Materials Branch in anticipation of the acceptance of the program and numerous other members of the staff began to work intensively in the field of glass science. The result has been an active and closely coordinated group involving materials prepration, experiment, and theory. Detailed results obtained in the alkali halide and glass programs are discussed.

The long term objective of the program on refractory metals was the preparation and study of highly perfect specimens in which the only structural feature was a grain boundary of controlled misorientation. To achieve this purpose it was necessary to develop techniques for the production of highly perfect single crystals and for joining them to make bicrystals of controlled-misorientation. Program accomplishments have been made in five areas: (a) growth of single crystals of niobium; (b) characterization of single crystals by X-ray techniques; (c) optical observation of dislocation structures; (d) sintering of intergranular porosity; and (e) grain boundary self-diffusion in bicrystals.

Major progress in the program on transition metal and intermetallic compound single crystals included: (a) development of methods for applying high-resolution electron microscopy to the study of metallic crystal growth; (b) development of mathematical procedures for theoretical analysis of time-dependent crystal growth during embryonic stages of growth in both supercooled and hypercooled melts; (c) the first kinetic measurements of crystal growth in a hypercooled melt, which lead to a unique analysis of dendritic growth at extreme levels of supercooling; (d) establishment of a new theoretical approach for determining atomic attachment mechanism for crystal growth in metals, semiconductors and congruently-melting intermetallic compounds; (e) measurement of the thermal conductivity of high-purity rhenium and palladium from 2-20°K showing the existence of a new electron-electron collision term for the thermal conductivity of these metals; (f) the first experimental verification of the presence of electron-paramagnon scattering in high-purity palladium; and (g) the determination to high precision of the neck-orbit dimensions for the Fermi surface of high-purity copper via magnetoacoustic techniques.

In the program on the crystal synthesis and characterization of magnetic materials, progress in the synthesis area included construction of a vacuum single crystal furnace for avoidance of oxidation during crystal growth, partial construction of apparatus which will permit pretreatment of fluoride starting materials in HF to eliminate hydrate oxide and basic salt impurities, and the preparation of a series of α Al_2O_3 single crystals doped with Fe^{3+} at different concentration levels. Progress in the area of characterization included: (a) optical absorption studies of K_2CoF_4; (b) ESR studies of single crystals of K_2ZnF_4 doped with Mn^{2+} and single crystals of K_2ZnF_4 doped with Fe^{3+}; and (c) optical and ESR studies of single crystals of α-Al_2O_3 doped with Fe^{3+}.

BEST AVAILABLE COPY

AUTHORIZATION

NRL Problems P03-07, P02-02, M01-09 and M01-10 - ARPA Order 418

PROBLEM STATUS

This is an interim annual report; work continues on various aspects of these problems.

ALKALI HALIDE CRYSTALS

GLASSES

Personnel Engaged in Program

J. Allard
R. Black
R. J. Ginther
H. S. Goulart
M. Hass
C. C. Klick
R. Kirk
M. Krulfeld
A. R. Ruffa
G. Sigel
J. H. Schulman, Project Scientist

Report Prepared by: C. C. Klick and M. Krulfeld

I. INTRODUCTION

During the past year the work undertaken has fallen into two major categories. For the first portion of the year work continued on the alkali halide crystal problem, and included further development of methods of purification of the raw materials, methods of crystal growth, and analysis of the final product. In particular, several projects within the Optical Materials Branch were appreciably aided by the resources developed in this program.

Several months after the beginning of the report year a proposal was made to enlarge in a very substantial way the effort going on in glasses and to emphasize the research aspects concerned with understanding the most fundamental properties of glass. Approval of this plan came near the beginning of the present calendar year and the character of the work has changed dramatically in the last portion of the year. Three new members have been added to the staff of the Optical Materials Branch in anticipation of the acceptance of the program and numerous other members of the staff began to work intensively in the field of glass science. The result has been an active and closely coordinated group involving materials preparation, experiment, and theory. In discussing the work below, no separation will be attempted between the work on crystals and that on glasses. It should be evident in each section as to which material is being discussed.

II. MAJOR NEW FACILITIES

Two adjacent clean rooms have been built in laboratory space between the zone-refining and crystal-growing laboratory and the room housing the mass spectrograph. The entrance to the clean rooms is through an entrance port in the crystal-growing area. An additional pass-through port is located between one of the clean rooms and the mass spectrograph room to permit preparation of samples in the clean area for mass spectrograph analysis. A White Bench is located in each of the clean rooms to provide an ultra-clean space. Clean-room work benches and storage facilities for pure materials are provided in each room. Clean-room protective garments are provided for all work in the clean area. It is anticipated that use of this facility will greatly increase the ultimate purity of raw and final product materials which can be attained.

There is now in operation an elegant and unique glass furnace which has been designed and produced by the Arthur D. Little Co. f... Dr. Ginther. It allows for the heating by induction of a glass melt in a crucible enclosed within a vacuum chamber. Melting can be accomplished either in a vacuum, oxidizing atmosphere, reducing atmosphere, or inert atmosphere. It allows for all the glass handling operations to be carried on within the controlled atmosphere. These include filling, melting, stirring, casting, and annealing. It is the first furnace of this kind to have been made and as a result it has needed a great deal of adjustment and modification. However, it is now

BEST AVAILABLE COPY

operating satisfactorily and has already proved its worth in one of the research projects which will be described later. With the aid of this furnace it has been possible to prepare a sample of simple sodium-silica glass with extremely small concentrations of iron impurities. The improvement over glasses melted in the usual glass furnaces has been quite impressive.

Equipment has been assembled for Raman spectroscopy. It consists of a 50 milliwatt helium-neon laser and a Spex double grating monochromator. Detection is accomplished either by using a photomultiplier with a phase sensitive detector or with a discriminator and counter. The apparatus has been assembled, aligned, and preliminary spectra have been obtained using liquids and glasses.

Appropriations have been approved for the addition of two other pieces of apparatus. One is an apparatus for preparing thin films by sputtering; the other is an interferometric spectrometer for use in the far infrared.

In addition to facilities within the Optical Materials Branch, cooperative effort has been begun with other groups at NRL that have unusual facilities. Mr. W. R. Hunter of the Atmosphere and Astrophysics Division has contributed his time and extensive vacuum ultraviolet equipment and is starting a program of reflection and transmission measurements on glasses. Similarly, Dr. G. A. Ferguson, Jr. of the Nuclear Physics Division has used the NRL reactor and neutron spectrometers to demonstrate the feasibility of studying the structure of glasses using this equipment.

III. MATERIAL PREPRATION AND ANALYSIS

A. Alkali Halide Purification and Single Crystal Preparation

Alkali halide purification and zone-refining was delayed by construction work on clean-room laboratory space over a portion of this period. While the zone-refiner was not in operation a number of modifications, such as very pure hydrogen halide gas generating apparatus, an improved vacuum handling system, and the like, were designed and fabricated for the equipment. It is presently being employed to prepare highly purified RbCl for conductivity studies. The zone refiner has also been used to prepare a zone-levelled KBr ingot doped with multiple impurities. After analysis it will be used as an impurity calibration standard for analyses of trace impurities in ultra-pure KBr, particularly by mass spectrography. A single crystal of KBr, doped with 0.02 percent of NaF, LiBr, RbCl, CsBr, KI, $CaCO_3$, $SrBr_2$, $BaCO_3$, $MgCO_3$, $PbBr_2$, AgBr, $AlCl_3$, KNO_3, SiO_2, and $MnCO_3$ respectively was also prepared by Kyropoulos crystal pulling and has been analyzed by a variety of techniques for us by C. Butler of ORNL to provide a standard. Different portions of this single crystal differ markedly in impurity concentration, indicating the desirability of having a larger, more uniform zone-levelled ingot as standard.

Papers have been written and published on KBr crystal growth by vapor deposition(1) and on a laboratory method for making Teflon to glass

BEST AVAILABLE COPY

connections.[2]

B. Purification Analysis and Preparation of Glasses

For studies of the optical properties of iron-containing lithium and sodium silicate glasses, the analysis of small amounts of iron in raw materials used to prepare such glasses and the purification of such raw materials became of interest. As part of this work R. Black adapted a standard colorimetric technique for the analysis of Fe in Li_2CO_3 and Na_2CO_3 with good accuracy down to the fractional ppm level with an uncertainty of ±0.2 ppm Fe. The method involved formation of a ferrous complex with Bathophenanthroline (4-7 Diphenyl, 1-10 Phenanthroline) and extraction of the complex into iso-amyl acetate or chloroform, with absorption spectrophotometry to determine the amount of complex formed. One lot of reagent grade Na_2CO_3 containing less than 1 ppm of Fe was found to be available. The available reagent grade Li_2CO_3 contained heterogeneously distributed Fe in a much higher amount (several ppm). It was possible to reduce the Li_2CO_3 content of Fe by several methods to approximately 1 ppm--ion exchange, recrystallization, and by filtering a water solution through a 0.45μ pore-size Millipore filter. In the course of the filtering work it was found that very fine particulate matter present in the reagent grade Li_2CO_3 not only contained a 50% or larger portion of the iron present, but also acted as an absorbent or ion exchanger for Fe when it was added as an impurity in small amounts (4 ppm) as a soluble compound. The added impurity, on filtration, did not appear in the filtrate, but was found on the filter. The nature of the solid particles is not known at present. By using very pure HF to dissolve pure SiO_2 powder, previously prepared by R. Ginther, and analyzing the resultant solution for Fe by the Bathophenanthroline method it was shown that different samples of the SiO_2 varied in iron content from about 0.3 to 1.6 ppm, with an average of 0.8 ppm.

In the study of sodium silicate glasses which will be described later in this report, it was found that the Fe^{3+} content of these glasses could be obtained in various ways. By grinding a standard size sample of glass and measuring the EPR spectrum intensity at g=4.28 with a Varian E-3 spectrometer, analysis of the Fe^{3+} concentration could be determined to better than 0.5 ppm. Optical measurements of the Fe^{3+} band at 225 nm could also be used to measure concentrations to about the same accuracy in the finished glass. This involved comparing the absorption spectrum against a blank prepared in a reducing atmosphere to convert any iron present to Fe^{2+}.

Although the raw materials had iron concentrations of about a ppm or less, glasses prepared in a normal glass furnace ended up with 6 to 8 ppm of iron. This furnace contained silicon carbide heating elements and was lined with the usual fire brick. It appeared, then, that the furnace atmosphere itself was a major source of iron contamination.

Glasses were then prepared in the special enclosed furnace where the crucible is heated by induction. Using the best raw materials and careful handling a glass was prepared with an iron content below the detection limits of the EPR apparatus which would place it less than 0.5 ppm of Fe^{3+}. As a

BEST AVAILABLE COPY

result it has been possible to investigate separately the transmission of the base glass and the effect of iron impurity on the ultraviolet transmission of the sodium silica glass.

C. Characterization by Mass Spectrography

A major portion of our characterization work has been on the utilization of our RF spark source mass spectrograph for the analysis of alkali halides and glasses, and the development of techniques for handling these and other dielectrics for useful qualitative and quantitative analyses

A Fortran computer program has been set up to calculate concentrations of impurities from an input of data obtained by densitometric measurements of peak height and background. The program has been used successfully for KBr, CaF_2, LiF, and several glasses. A first draft describing the program has been written (J. G. Allard and P. Bey) and is presently being revised. Use of the program has resulted in a reduction of at least 90% in the time required to make the necessary calculations after identification and densitometry on the photographic plate, and has, in addition, drastically reduced the possibilities of unrecognized errors in such calculations. Finally, it computes the minimum detectable concentration as well as that observed so that estimates of accuracy can be more precise.

The program was used first to check and recalculate data available on the backlog of plates from previous mass spectrographic analyses, particularly of KBr, as well as other alkali halides. Some of this data has been presented in a paper[3] in which the techniques employed and some of the difficulties encountered in attempts to achieve adequate calibration for quantitative measurements have been described.

A technique for increasing the conductivity of alkali halides and of glasses was developed by J. G. Allard, consisting of irradiation of samples to be analyzed by a beam of 2 Mev electrons. While too low in energy to produce radioactive isotopes which could deposit in the spectrograph and cause interference by later affecting the photographic plate, the radiation generates vacancies in alkali halides and in glasses, and permits solid samples of these materials to ionize readily in the R. F. spark source of the instrument. Samples of KBr crystal analyzed by this technique appear to give a better mass spectrum than that previously obtained by direct treatment in the R. F. source without the radiation treatment. A variety of glasses, chiefly sodium silicate glasses, have readily produced an ion beam in the instrument after the electron beam treatment. The mass spectrum from glasses varies in quality from run to run, but appears to be quite adequate for qualitative analyses, with sensitivities below 1 ppm for most of the elements observed. However, the ionization efficiencies for different elements in glasses varies markedly, and the ionization efficiency ratios are not constant for the elements from run to run. It appears that small differences in sample geometry and other sparking factors affect the ionization efficiencies in the less conductive materials even after the radiation treatment, in contrast to inherently more conductive materials such as metals. Only semiquantitative analyses are presently possible with the method, which would need extensive standardization and calibration studies for improvement. Pending such studies, work is presently underway with mixtures of conductive pure graphite powder with powdered samples of glasses, the mixtures being pressed into solid tablets and sticks under high pressure. The high conductivity of the mixture should give more reproducible results, at the price of lower sensitivities and increased contamination. Such results will permit more accurate quantitative analyses at impurity levels presently needed in the glass program. Initial results are promising. An auxiliary technique for mounting alkali halide materials on an electrically heated gold or platinum wire in a clean inert gas environment has been developed and may now also prove useful in mounting mixed graphite and alkali halide powder. An improvement in the instrument background, particularly for Fe, Ni, and Cr has been made by substituting tantalum parts for steel and stainless parts and by shielding portions of the source housing.

IV. RESEARCH PROGRAMS

A. Optical Properties of Glass in the Vacuum Ultraviolet

With the cooperation of Mr. Hunter of the Atmosphere and Astrophysics Division steps have been initiated to do an elaborate and rigorous study of crystalline quartz, fused silica and simple glasses using the two angle reflectivity method and to make this investigation as precise and accurate as is currently possible in this wavelength region. Also work is in progress to adapt a low temperature dewar to the vacuum UV spectrometer so that the facilities can be adapted for measurements other than those at room temperatures. Mr. Hunter, Dr. Hass and Mr. Sigel have done a preliminary study of the reflection spectra of high purity Corning No. 7940 fused silica at one angle and at room temperature. The results obtained show very clearly the presence of two peaks in the reflection spectra of fused silica. One is at 10.3 ev and the other at 11.5 ev. These peaks agree almost exactly with those which have been reported for crystalline quartz (E. Loh, Solid State Comm 2, 269(1964)).

More recently measurements have been reported on crystalline quartz and fused silica still further into the ultraviolet (H. R. Philipp, Solid State Comm. 4, 73(1966)). A nearly identical spectrum of four bands is found in each case.

Dr. Ruffa has considered these results from the point of view of molecular chemistry and has looked into the possibility of simple explanations of the vacuum ultraviolet reflection peaks. A manuscript describing these results has been submitted for publication.(4) The similarity of the fused silica and crystalline quartz would indicate that the processes involved are not strongly dependent on the presence of long range order but that more localized effects predominate. The sharp peak at 10.1 ev in quartz has been identified as a Wannier exciton formed by the breaking of a single Si-O band. The next broad peak is attributed to the conduction band, the bottom of which is at about 11.3 eV. A barely resolved hump in Loh's data at 12.5 eV has been associated with a molecular exciton formed by the breaking of two Si-O bands and the demotion of the Si atom back down to its ground state. The next broad peak has been identified with two unresolved molecular exciton bands formed by the promotion of an O atom to either a ^5S state or a ^3S state and the weakening of an Si-O band. Finally, the last broad band observed by Philipp beginning at 17 eV has been associated with a series of molecular exciton bands involving further excitation of an O atom. These are presumed to merge into each other and into the next conduction band beginning at about 20 eV. The implication of these results with regard to the valence band treatment of other crystals and disordered glassy materials is also discussed.

Dr. Ruffa is currently active in making somewhat more fundamental calculations which involve less reliance on empirical data. Eventually, of course, one should look into the additional effects introduced by the presence or absence of long range order on these processes. But the establishment of a simple physical model for the principal optical absorptions in the ultraviolet appears to be an extremely important foundation stone for further unraveling of optical processes.

Reflection measurements have also been obtained on simple sodium silicate glasses. The results are not entirely reliable because of the possibility of water vapor attack on the surface of this glass. However, the lowest two energy peaks seen in fused silica are seen again, as well as a new peak at still lower energy. These measurements will be repeated on samples specially prepared and handled to avoid the moisture problem.

At energies between 6 and 10 eV there is strong absorption in complex glasses but relatively weak reflection. For this energy range, which appears to be promising for unravelling the electronic properties of complex glasses, transmission measurements on thin films appear to be the best experimental solution. Mr. Sigel plans to take this investigation on as a thesis problem.

Mr. Sigel and Mr. Ginther have been actively at work in the near ultraviolet (2000-3000A) region of the spectrum--that which is closest to the transparent region of most glasses. Such glasses are opaque in the "near-ultraviolet", but it is known that some glasses can be made to be quite transparent in this region also. Usually the technique involved is to prepare glasses of reasonable purity and to melt them under reducing conditions.

A variety of suggestions have been made as to the origin of the absorption in this wavelength region. Because of the effect of the reducing atmosphere one could imagine that the absorption arises from the incorporation, in some way, of atmospheric oxygen as an excess into the glass. On the other hand, the universal presence of contaminants in the usual glasses suggest the alternate possibility that some metal ion is undergoing a valence change which changes its absorption characteristics. Both of these explanations have been proposed in the literature.

Mr. Sigel and Mr. Ginther have now completed an initial study on the simple sodium silicate glass made with as high purity as we are capable of producing at this point. The glass was also made with additions of iron impurities in the range up to 1000 ppm, and was fired under both oxidizing and reducing conditions. Optical measurements have been made both in samples of usual thicknesses--about 1 mm--and on samples ground down to thicknesses of only 40 microns. In addition electron paramagnetic resonance measurements have been made on these glasses to ascertain an independent measure of the amount of Fe^{3+} that may be present. The results seemed to indicate that while the raw materials used may have had iron concentrations of as little as 1 part per million, the finished glass runs between 5 and 10 parts per million even under extremely careful conditions of preparation. This would imply that the more ordinary procedures which have generally been used in preparing glasses for investigations in this region would lead to iron concentrations which are considerably higher. It is learned furthermore that the Fe^{3+} puts in an absorption band which appears to peak in the region close to 2250A and this peak can be followed even at very high iron concentrations introduced in the heavily doped samples. However, this peak can only be measured in extremely thin samples because of the very large absorption coefficient which results. For samples of more ordinary size the absorption band would appear as a shift of the "fundamental edge" which has on occasion been reported. These experiments do not indicate any change at all in the absorption in the region of 2000A due to the presence of Fe^{3+}. Thus it appears that Fe^{3+} does indeed introduce a very strong absorption in the near ultraviolet region and that for glasses of only average purity the iron absorption may give rise to the well known near ultraviolet opaqueness of glasses. In addition the investigations of the purest glasses show only a very small difference between glasses produced in oxidizing and reducing conditions. This result argues that, in these glasses at least, the firing under oxidizing conditions does not introduce an appreciable amount of excess oxygen which leads to optical absorption. A manuscript describing this work has been prepared.(5)

There are several intriguing aspects of the iron problem in relation to practical glasses. Soda lime glasses used in windowpanes are only slightly more complex than the sodium silicate glasses investigated here in that some calcium is added. It seems entirely likely that such a glass would be transparent to near ultraviolet if it were made free of iron. We hope to look into this. If this were the case, it may be possible to make U.V. transmitting glasses, windows, and prisms using ordinary glass recipes and melting in air but using materials of high purity.

Preliminary studies here of the radiation effects of ultraviolet light on laser glasses also suggest that iron impurities may play a role. If Fe^{3+} is present and is changed to Fe^{2+} by the Xenon lamp radiation, one might expect several optical changes. First, the Fe^{3+} absorption band at 2250A would decrease as is observed. Second, this process would leave excess holes which form visible absorption bands as is also observed. Finally, the

BEST AVAILABLE COPY

Fe^{2+} forms a strong quenching center for many laser ions in glass and this would tend to reduce the laser efficiency as is also observed. The possibility that this mechanism is an important one is being studied further.

There are a number of other research areas in which important contributions have been made by materials or analyses supplied as a result of this program. Analysis of pure Harshaw LiF and the Harshaw thermoluminescent dosimeter material TLD-100 established that not only Mg was present but also Si, P, Mn, and O most of which had not been previously detected.(6) Furthermore the absence of Ti eliminated a previously published suggestion that it was the luminescence center.

Various kinds of analysis of normal Harshaw CaF_2 and "rare earth free" CaF_2 also from Harshaw showed that ineed the "rare earth free" material was purer in that respect but that it contains 35 ppm of Mn. The coloration properties of the "rare earth free" CaF_2 have been studied(7) and the EPR and ENDOR properties of the Mn in CaF_2 are presently being pursued.

Recent studies here on ionic conductivity of RbCl in the intrinsic range have shown curvature that has been analyzed as due to contributions from both anions and cations(8). However, the activation energy for the halide ion has an anomalously large value. Further studies are planned using zone refined RbCl which will extend the intrinsic region over which measurements can be made as well as RbCl doped with divalent metal impurities. These special crystals are being prepared here.

V. FUTURE PLANS

The reflectivity measurements in the vacuum ultraviolet will include careful two angle measurements on pure fused silica and various cuts of quartz. Measurements may also be extended to GeO_2 for which the theory should also be applicable with minimal modifications.

Attempts will be made to place the theory on a more fundamental basis with less reliance on empirical observations. Hopefully the concepts may be extended to more complex glasses such as the sodium silicates.

Vacuum ultraviolet transmission measurements will be attempted on blown and sputtered films of simple glasses such as silicates with additions of Na, K, Li, Al, and Ca. It is hoped to be able to identify the electronic transitions and from these to understand the bonding of these ions in the silicate matrix.

Neutron diffraction will also be studied on these simple glasses since it gives more detailed information than x-ray diffraction does. It has been observed elsewhere that the first x-ray peak in the radial distribution representative of the Si-O distance is altered as the sodium concentration increases. Attempts will be made to understand this and other peak structure in relation to the structure of glass.

Raman and far infrared spectra will be taken on SiO_2 with trace additions of alkali and alkaline earth ions. This will also aid in determining the bonding and placement of these ions in glasses by analysis of their vibrational spectra.

Other studies which are contemplated center around the problem of coloration of glass by radiation. The nature of these color centers is not known except that it is believed that two of them in the visible region of the spectrum involve holes. Studies of the time and temperature dependence of coloration both in pure glasses and in glasses "protected" by Ce, Cl_2, H_2 or other ions should yield information about the coloration and protection mechanisms. It is hoped that a similar study of the coloration in photo-chromic glasses will aid in understanding coloration in those materials.

Two post doctorate students, experience in glass research, will join the Optical Materials Branch this fall. Dr. Anderson of Illinois plans to study the optical properties of MgO:V both as a crystal and a glass and hopes to unravel the differences in structure from a detailed analysis of the spectrum. Dr. Griscom of Brown University has studied the V_K center in halogen doped glasses as well as the EPR results on Mn^{+2} in glasses. Studies here will continue in these directions.

VI. COOPERATIVE PROGRAM WITH BAUSCH AND LOMB AND PENN STATE

Contract negotiations between ONR and Bausch and Lomb were completed near the end of this reporting period--to establish a complementary program of glass research there. The major areas of cooperative effort between NRL and B+L during the first year are to be:

1. Exchange of raw materials and analyzed samples. This is intended to compare analysis by mass spectrography (NRL) with careful analysis by emission spectrography (B+L). Furthermore it will serve to compare the impurity problem of quite different sources of raw materials.

2. Samples of fused silica will be prepared with additions of small quantities of various alkalis. Cooperative measurements using vacuum ultraviolet spectroscopy, far infra-red, and Raman spectroscopy will hopefully indicate how alkalis are built in to glasses in the simplest cases.

3. Preliminary to the procurement of our own sputtering facilities, sputtered films of glasses will be prepared for study.

4. A review will be prepared of some field in which B+L has special competence and which is of interest to NRL.

In addition it is anticipated that B+L studies on the effect of excess oxygen in glasses will continue and form an important part of the overall program.

A meeting of active glass scientists from Penn State, Bausch and Lomb, and NRL was held at NRL. Discussions were held on current research activities in each group, and there was a reasonably detailed exploration of areas in which each group could profit from interaction with the others. NRL-B+L contact has been described above. Penn State has unique facilities for splat cooling and for diffusion of gases into glasses at high temperatures and pressures. NRL was especially interested in the possibility of making glasses of ionic solids such as alkali halides by the splat cooling process. In addition the possibility of making protected glasses by diffusing of H_2 and Br_2 was of interest. Ce protected glasses do not protect instantaneously but have a time constant of about 0.1 second. Studies of other protected glasses would be of interest both for practical applications and to determine the mechanism of protection for the various protecting ions. It is hoped that cooperative work in this area will be carried out in the coming year.

REFERENCES

1. "KBr Growth by Deposition from the Vapor", M. Krulfeld, Mat. Res. Bull. 2, 337(1967).

2. "A Laboratory Method for Teflon-to-Glass Connections", M. Krulfeld, J. Chem. Ed. 44, 303(1967).

3. "Impurity Analyses of Alkali Halides by Mass Spectrography", J. G. Allard and M. Krulfeld, Mat. Res. Bull. 2, 419(1967).

4. "The Valence Bond Approximation in Crystals:Application to an Analysis of the Ultraviolet Spectrum in Quartz", A. R. Ruffa, submitted to J. Phys. Chem. Solids.

5. "Ultraviolet Absorption of Soda-Silicate Glass", G. H. Sigel, Jr. and R. J. Ginther, to be submitted to Physics and Chemistry of Glasses.

6. "Thermoluminescence and Color Centers in LiF:Mg", C. C. Klick, E. W. Claffy, S. G. Gorbics, F. H. Attix, J. H. Schulman, and J. G. Allard, to be published in J. App. Phys.

7. "F Band in X- and Electron-Irradiated CaF_2", D. A. Patterson and R. G. Fuller, Phys. Rev. Lett. 18, 1123(1967).

8. "Anion Contributions to the Electrical Conductivity of Alkali Chlorides", R. G. Fuller and M. H. Reilly, Phys. Rev. Lett. 19, 113(1967).

TRANSITION METAL AND INTERMETALLIC COMPOUND SINGLE CRYSTALS

Personnel

Principal Investigators:	A. I. Schindler
	M. E. Glicksman
	G. N. Kamm
	R. J. Schaefer
	J. T. Schriempf
	C. L. Vold

I. INTRODUCTION

The program over the past (and terminal) year produced a number of significant scientific developments. In many respects, the progress over this reporting period can be considered as the culmination of the efforts expended over the earlier years of the program where impetus was gained through progress in the areas of crystal preparation and characterization of purity and perfection.

Specifically, our ability to prepare and characterize high-purity palladium, in large measure permitted the first experimental demonstration that electron-paramagnon interactions do exist in certain pure transition metals and, at low temperatures, account for some of the behavior of these materials. Also, the preparation of high-purity rhenium crystals by ultra-high-vacuum electron-beam zone refining allowed a detailed investigation of the low-temperature thermal conductivity of this material. This investigation was conducted at temperatures where, with less pure specimens, electron-impurity interactions would have completely masked the effects of interest. These examples also serve to show that as crystalline purity and perfection improve, entirely new phenomena can be uncovered, and known phenomena can be investigated in regions of temperature previously precluded by the interfering effects of point, line, surface, and chemical imperfections.

Our understanding and outlook concerning crystal growth processes has similarly improved over the past year. New methods for investigating atomic attachment processes--the fundamental step, repeated over and over during the growth of a crystal--have been developed, which, for the first time, will permit these investigations in metal and semiconductor crystals. The application of electron microscopy toward in situ crystal growth studies has been developed as an extension of the optical studies performed in 1965 at NRL. The promise is now held out that defect incorporation during crystal growth can be observed and, perhaps, ultimately controlled at the near-atomic level.

Finally, new types of crystal growth, such as solidification of hypercooled melts, have been discovered and then analyzed both experimentally and theoretically. The major accomplishments of the past year are listed below:

1) Developed the methods for applying high-resolution electron microscopy to the study of metallic crystal growth.

2) Developed the mathematical procedures for theoretically analyzing time-dependent crystal growth during embryonic stages of growth in both supercooled and hypercooled melts.

3) Obtained the first kinetic measurements of crystal growth in a hypercooled melt, which lead to a unique analysis of dendritic growth at extreme levels of supercooling.

4) Established the theory of a new approach for determining the atomic attachment mechanisms for crystal growth in metals, semiconductors, and in congruently-melting intermetallic compounds.

5) Measured the thermal conductivity of high purity rhenium and palladium from 2°-20°K and showed the existence of a new electron-electron collision term for the thermal conductivity of these metals.

6) Established the first experimental verification of the presence of electron-paramagnon scattering in high purity palladium.

7) Determined to high precision the neck-orbit dimensions for the Fermi surface of high-purity copper, via magnetoacoustic techniques.

II. GROWTH OF METAL SINGLE CRYSTALS

A. Electron Microscopy of Metal Crystal Growth

Techniques have been developed which permit observation of melting and freezing phenomena within an electron microscope, as well as observation of static, equilibrated solid/liquid interfaces at high magnifications (above 10,000 X).

Thin polycrystalline films of pure bismuth were prepared by vacuum evaporation onto a 100 Å film of amorphous carbon; the latter was supported by standard 100-mesh electron microscope grids. Controlled melting of a film was accomplished by maintaining the temperature of the microscope's heating stage about 20° to 30°C below the normal melting temperature, and then relying on the heating effects of the focused electron beam to induce melting over the very localized areas ($\sim$ 60 microns^2) under observation. Melting and freezing could be controlled easily using these techniques, and very stable solid/liquid interfaces could be maintained almost indefinitely for study at high magnification.

Figure 1 shows the effects of a grain boundary on a slowly advancing solid/liquid interface. Note that while the dihedral angles of the tri-junction remain substantially constant over the time interval between photographs (approximately 30 seconds), some boundary motion toward the right is visible in Fig. 1(b). Furthermore, the solid/liquid interface has advanced downward (on the photograph) and become nearly straight in both grains; this implies that crystallographic faceting on a microscopic scale is occurring in bismuth during solidification--an observation which seems to be in accord with a recent theory of solid/liquid interfaces.[1]

Another interesting phenomenon, observed for the first time, is shown in Figs. 2 and 3, where microscopic "pools" of molten bismuth are equilibrated within a single crystal. Although nearly circular pools could have formed had the pools been of ordinary macroscopic dimensions, instead, polygonal areas of liquid formed, which were surrounded by faceted borders having a direct crystallographic relationship with the surrounding crystal structure. The reasons for the formation of these faceted pools are not certain at this time, but the phenomenon could be explained on the basis of an anisotropy in the solid/liquid surface energy.

Further experimental work is now underway to explore these effects further and, perhaps, extend this technique to motion picture studies of kinetic effects during melting and freezing.

B. Growth Rate of Spherical Crystal Nuclei

When a crystalline material grows into a pure supercooled liquid, the rate of growth of the crystal is a function of the supercooling at the crystal/liquid interface, i.e., of the difference between the actual crystal/liquid interface temperature and the local crystal/liquid equilibrium temperature. The local crystal/liquid equilibrium temperature is a function of the curvature of the interface, and for strongly curved interfaces may differ by many degrees from the familiar thermodynamic melting temperature. Moreover, the actual temperature of the crystal/liquid interface is determined in part by the heat diffusion field of the latent heat of fusion emitted by this interface as it advances during solidification. The function relating growth velocity to interface supercooling depends upon the specific kinetic mechanism of atomic attachment at the crystal/liquid interface.

Numerous papers published in recent years have considered the temperature distribution about solidifying bodies growing in supercooled liquids. However, none of the available studies in the literature demanded that the interface temperature-interface velocity relation be consistent with both heat flow and atomic kinetics.

Equations have been derived representing a geometrically simple but physically significant solidification problem; these equations relate the interface temperature to the interface velocity through both a kinetic relation and the heat diffusion equation. Moreover, the effect of curvature on equilibrium temperature is fully accounted for and is of great importance.

The process under consideration is the growth of a sphere of solid in a supercooled liquid. The sphere is initially of such a small size that surface curvature effects depress its equilibrium temperature to the temperature of the supercooled liquid. The problem under consideration was to determine the subsequent growth behavior of the spherical nucleus when its metastable equilibrium is upset by introducing a small perturbation into the radius.

The incorporation of atoms at the solid/liquid interface is described by a differential equation relating the growth rate of the solid sphere to the radius and interface temperature. Simultaneously, an integral equation relates the interface temperature change to the emission and diffusion of latent heat resulting from this growth. Solutions of these coupled equations, generated by the CDC 3800 computer, give the radius and growth rate of the sphere, and the temperature at the surface of the sphere, all as functions of time. These solutions show that the growth velocity of the spherical nucleus passes through a maximum and then declines, as shown in Fig. 4.

The physical constants used for the calculation were those of white phosphorus, since crystal growth in supercooled liquids of this material has been the subject of recent investigation. Supercoolings are expressed in units of the dimensionless parameter $\Phi = C\Delta T/\lambda$, where C is the specific heat of the liquid, λ is the latent heat of fusion, and ΔT is the temperature difference between the bath temperature and the thermodynamic equilibrium temperature. The growth rate in this material reaches a maximum in a very short time, and then decays to a steady-state value which is zero for $\Phi \leq 1$, and is greater than zero for $\Phi \geq 1$.

The computer solutions of the sphere problem, as described above, represent the earliest stages of crystal growth following nucleation in a supercooled liquid. It is expected that the growing sphere will eventually develop instabilities which will grow into dendrites; the relation between the maximum calculated growth velocity for spheres and the measured velocity for dendrites is currently under investigation. The calculations are also being extended to apply to metallic systems which have much greater themal diffusivities.

C. Analysis of Crystal Growth Kinetics Using Peltier Thermal Waves

The rate of crystal growth, v, at a solid/liqu interface is related to the supercooling of the interface, ΔT, by a function which is determined by the atomic attachment mechanism. Hence, measurements of the kinetics of solidification would indicate which of the several possible attachment mechanisms actually operate in a particular system under study. In addition, quantitative determinations of the kinetics of solidification are important in understanding the development of the complex morphologies assumed by growing crystals. In metallic systems, most experimental techniques for measuring interface supercoolings have failed due to the unavoidable combination of small interface supercoolings, rapid growth rates, and steep temperature gradients. Over the past few years, an oscillating interface method[2] involving the study of periodic interface motions and temperature variations has been used, but with only moderate success. We have now developed an alternative method which will overcome some of the experimental and analytical difficulties of the original oscillating interface experiment; the new method is particularly suited for the determination of solidification kinetics in metals and semiconductors.

Periodic Peltier heating and cooling may be generated at a metal or semiconductor solid/liquid interface by the passage through the interface of an alternating electric current. A new method for the measurement of solidification kinetics has been developed in which an oscillating interface motion is produced by the Peltier effect, and the rate of this motion is measured electronically.[3] (See Fig. 5.) The temperature variations of the interface can be calculated from a knowledge of the net interface heat emission, which is the time-varying algebraic sum of the Peltier and latent heat emissions; the former (input heat flux) is proportional to the electric current, and the latter (response heat flux) is proportional to the measured rate of interface motion. Hence, simultaneous measurements of the electric current and the interface velocity yield sufficient data to determine the interface velocity-temperature relation from which, in turn, the attachment mechanism can be deduced. The waveform of the resulting interface motion can then be analyzed with a high-speed digital computer to determine the kinetic law relating interface velocity to interface temperature.

Depending upon the mechanism of atomic attachment at the solid/liquid interface, the form of the kinetic law (v as a function of ΔT) describing the growth of a metal crystal might be linear, parabolic, or exponential. The new experiment, unlike previous oscillating interface methods, is applicable to nonlinear as well as linear kinetics. Moreover, we are able to describe in advance the response expected from an interface displaying any of these kinetic laws, and have obtained computer-generated curves showing the motion of interfaces with linear, parabolic, and exponential kinetics. As examples, Figs. 6a, 6b, and 6c show waveforms of interface motion in systems subjected to square-wave Peltier heat inputs. The computed curves indicate that the different kinetic laws will result in distinguishably different waveforms of interface motion. An investigation of the solidification kinetics of mercury, bismuth, and gallium utilizing the technique described above is now underway.

D. Dendritic Crystal Growth at Large Supercoolings

Attempts to measure the deviation of interface temperatures from equilibrium in metallic systems have invariably been vitiated by the large temperature gradients which are associated with the release of the latent heat of fusion at a moving interface. Thus, the many published measurements of dendrite growth velocities in supercooled liquids provide little information directly concerning the atomic kinetics of solidification, because, although bath supercoolings are measured, the <u>interface</u> supercoolings still remain unknown.

In theoretical analyses of the heat flow near a dendrite tip, it is usually assumed that the interface supercooling is only a small fraction of the total bath supercooling, which implies that only small interface supercoolings are required to produce large solidification velocities. This assumption has appeared reasonable until now because there had been no demonstration that the interface supercooling in rapidly growing dendritic systems was ever, in fact, more than a very small fraction of the total bath supercooling. It will now be demonstrated that in at least one substance (P_4) the assumption of small interface supercooling is incorrect.

The normal end product of rapid dendritic solidification in supercooled melts is a two-phase slush of solid and liquid material at the thermodynamic equilibrium temperature. It was recently demonstrated, however, that when a critical bath supercooling is exceeded, the supercooled melt solidifies to a single-phase, totally solid, material.[4] Moreover, this final solid material is below the equilibrium melting point by an amount

$$\Delta T_f = \Delta T_b - \frac{\lambda}{C_p^{\ell}}, \qquad (1)$$

where ΔT_b is the initial bath supercooling, λ is the latent heat of fusion, and C_p^ℓ is the specific heat of the supercooled liquid; the minimum bath supercooling for total solidification is

$$\Delta T_b^* = \frac{\lambda}{C_p^\ell}. \qquad (2)$$

This minimum bath supercooling has not yet been attained in metals, but has now been achieved in liquid white phosphorus (P_4), a material in which solidification is expected to be similar to that of a pure metal, according to the theoretical criterion of Jackson.[5]

When crystal growth is initiated in a liquid supercooled beyond the minimum value given in Eq.(2), it then becomes possible to set certain limits on the temperatures attained by the solid/liquid interface. If the solidification proceeds through the hypercooled liquid as a planar front, it then follows from heat-flow theory that the temperature of the interface must be the same as that of the final solid product, and the interface supercooling is given in Eq.(1). If, instead, the interface breaks down during solidification into a non-planar configuration, then some parts of the interface will be supercooled more, and other parts supercooled less, than the value specified by Eq.(1). Furthermore, the coolest portions of the interface will be the most rapidly growing regions, which determine the observed solidification velocity. Thus, the value ΔT_f given by Eq.(1) represents the minimum possible interface supercooling at the fastest growing regions of the solid/liquid interface. It may be observed that this minimum interface supercooling becomes a significant fraction of the total bath supercooling, once the bath supercooling exceeds ΔT_b^*. Thus, if interface supercoolings are normally very small at bath supercoolings below ΔT_b^*, then greatly enhanced interface supercoolings, and hence enhanced solification velocities, should be produced at bath supercoolings above ΔT_b^*. In other words, a slope discontinuity of ΔT_b^* should occur in a plot of observed solidification velocity versus measured bath supercooling, if the interface supercoolings are small at low values of the melt supercooling.

Crystallization velocities in supercooled phosphorus have been measured at bath supercoolings above and below ΔT_b^*, i.e., in both supercooled and hypercooled melts. The phosphorus was contained in a 1 cm diameter vertical Pyrex tube (Fig. 7), and was protected from atmospheric contamination by a 0.5 weight-percent aqueous solution of chromic anhydride, which could be flushed through the liquid phosphorus column to cleanse the surfaces of the specimen. The tube was brought to a uniform temperature (within ±0.05°C in 10 cm) by immersion in a stirred water bath contained in a 2-liter Dewar vessel; the temperature of the specimen was measured with two calibrated tungsten-Kovar-A thermocouples using a precision potentiometer. The thermocouples were then connected in series opposed, and their output fed into a preamplifier and oscilloscope. The solidification velocity was calculated from the time interval, measured from the oscilloscope traces, required for the solidification front to traverse the 10-cm distance between thermocouples.

Figure 8 presents the results of the velocity measurements on a log velocity-log bath supercooling scale. It is seen that the solidification velocity is a smooth, continuous function throughout the entire range of bath supercooling. No sudden increase in solidification velocity occurs at bath supercoolings greater than ΔT_b^*, even though <u>interface</u> supercoolings become at least as large as 18°C. Since the velocity must be related to the interface supercooling, proportionately large interface supercoolings must have been present at bath supercoolings less than ΔT_b^*. Heat-flow solutions based on the <u>a priori</u> assumption that the solid/liquid interface is always near the equilibrium temperature may therefore be seriously in error in this system.

The study of this unique mode of solidification, thus far attained only in white phosphorus, has made it possible, for the first time, to set a lower limit on the interface supercooling during rapid dendritic growth. The implications of the velocity measurements with regard to interface morphology and the exact form of the kinetic relation are currently under investigation.

III. ELECTRONIC STRUCTURE AND PROPERTIES OF HIGH-PURITY METAL SINGLE CRYSTALS

Electron-Paramagnon Interactions in Palladium

It has been recently suggested[6,7] that, in strongly paramagnetic metals like Pd, a large renormalization of d-electron mass occurs as a result of d-electron-spin fluctuation interaction. The presence of such persistent spin-fluctuations (paramagnons) in the d-band can, as yet, only be inferred from a comparison of low-temperature specific heat data with heat capacities deduced from band calculations. However, a calculation for s-electron-paramagnon scattering has been made,[8] the results of which can be used as a means of verifying the existence of paramagnons in strongly paramagnetic metals.

To test this theory, and, indeed, to show that paramagnons do exist, low temperature electrical resistivity measurements were made on a series of dilute Pd-Ni alloys. Samples of pure palladium (having a resistance ratio $R_{300}/R_{4.2}$ in excess of 1000) and palladium containing 0.5, 1.0 and 1.66 at-% nickel were examined; the temperature region investigated was 2° to 30°K using conventional potentiometric techniques. Since these alloys do not exhibit any complicating localized magnetic moment phenomena,[9] it appears likely that the large increase in their magnetic susceptibility can be attributed to an increase in their exchange enhancement. As a result, we should expect that the fraction of the electrical resistivity resulting from electron-paramagnon scattering would increase strongly as a function of nickel content.

The results of this investigation are shown in Fig. 9. It is clearly evident that, at the lowest temperatures, the resistances of all the samples vary as T^2. For pure Pd, the observed electrical resistivity goes as T^2 to approximately 7°K; beyond that temperature a positive deviation is observed. As Ni is added to Pd, the coefficient of the T^2 term in the resistivity increases (note the upwards shift of ρ_i vs T on a log-log plot in Fig. 9), and in addition, the temperature region over which the T^2 dependence is observed is a strong function of the composition. For Pd-1/2%Ni, the resistivity goes as T^2 to 11°K; for Pd-1%Ni to 17°K; and for Pd-1.66%Ni to 5°K. The deviation from the T^2 behavior is found to decrease as a function of Ni content and, in fact, a negative deviation is observed for the Pd-1.66%Ni sample.

These results can all be explained by assuming that electron-paramagnon scattering is enhanced as Ni is added to Pd. One can write an expression for the ideal electrical resistivity in the following form

$$\rho_i = AT^2 + (B-C)T^5, \tag{3}$$

where A and C are the electron-paramagnon scattering terms and B is due to intra-band electron-phonon scattering. A and C can be theoretically related to the Stoner enhancement of the magnetic susceptibility. Thus the electron-paramagnon scattering is found not only to yield a T^2 term in the resistivity but also to attenuate the normal Bloch-Gruneisen T^5 term. Since, in the dilute Pd-Ni alloy system, the Stoner enhancement is found to increase as a function of Ni content, the coefficient of the T^2 term increases and, in addition, the attenuation of the T^5 term increases as well, as is observed. In fact, the electron-paramagnon contribution to T^5 is so large for the Pd-1.66%Ni sample, that a negative deviation from T^2 is observed beyond about 5°K.

B. Magnetoacoustic Oscillations in High-Purity Copper Crystals

The most elementary model for the Fermi surface of copper is a sphere--the free electron or Fermi sphere. A more realistic model takes account of the lattice periodicity and of the actual crystal potential. The detailed characteristics of the crystal potential will in most cases yield a Fermi surface substantially distorted from spherical form. In the case of copper, the sphere is distorted until it contacts the Brillouin zone faces in the {111} direction, creating "necks." Accordingly, the Fermi surface of copper becomes an open structure connected along {111} directions, and the open electron orbits which are made possible will profoundly influence some of the low temperature properties of the pure metal. A direct determination of certain Fermi surface cross sections in the vicinity of the necks may be obtained from analysis of magnetoacoustic oscillations and such measurements provide a valuable supplement to other experimental results concerned with the symmetries and shapes of the Fermi surface. Magnetoacoustic oscillations have been observed in a high-purity single crystal of copper which has opposite faces parallel to the ⟨110⟩ planes and which was spark cut from an ingot having a resistivity ratio of about 8000. The existence of necks limits the extent of "belly" orbits (those passing entirely around the Fermi surface) and makes entirely new types of orbits possible. These features produce a rich variety of magnetoacoustic oscillation patterns in which the effect of the necks can be seen in several ways.

1) A "shadowing" of belly-orbit oscillations occurs, i.e., in certain angular ranges (as indicated in Fig. 10) the belly orbits are blocked by the necks.

2) At angles successively closer to the {111} direction, groups of oscillations are observed representing orbits around 2, 3, 4...."Fermi spheres." Such extended orbits passing around as many as 10 "spheres" can be identified in the data.

3) "Geometric resonances" occur for the {111} direction; these arise when the periodicity of the orbit in real space is equal to a multiple of the sound wavelength. The specimen is pure enough that a series of eight such resonances occurs in the data. Since the periodicity of these particular orbits is directly related to the dimensions of the Brillouin zone, these data can be used as an accurate calibration for the magnetoacoustic oscillations, independent of the magnetic field value or the sound wavelength.

4) Magnetoacoustic oscillations arising directly from orbits around the necks are observed. Although their amplitude is reasonably large, an interpretation is made difficult by the presence of other oscillations having somewhat larger and smaller periods and arising from portions of larger, relatively complicated orbits.

An analysis of the neck-orbit oscillations in copper gave the pattern shown by the crosses in Fig. 10. Because their origin was clear, these data have been plotted from the center of the neck (point L) rather than from the center of the Brillouin zone, Γ. Superimposed, and shown as circles, are points derived from belly orbits for those angles where the latter are not shadowed by the necks and have sufficient amplitude. These points are plotted radially from the zone center. The dashed line is an analytic expression for the Fermi surface derived from Shoenberg's de Haas-van Alphen data by Roaf.[10] By the nature of Roaf's approximations, the fit is not good in the neck regions.

It is useful to compare the measurement of neck radii from the present experiment with the results from other measurements. Magnetoacoustic and magnetoresistance techniques are able to give this dimension directly in principal planes passing through the {111} axis and the results are given in Table 1. An <u>average</u> neck radius can be inferred from the de Haas-van Alphen measurement (which yield extremal areas) if it is assumed that the neck cross section is circular (which would be expected if the contact area with the Brillouin zone face were small). The average radial dimensions are shown in Table 1 for the data of Shoenberg[11] and for that of Joseph, et al.[12] For comparison, earlier magnetoacoustic measurements of Bohm and Easterling[6] have also been included.

The present magnetoacoustic measurements are in close agreement with the mean neck radius from the more recent de Haas-van Alphen data. This suggests that the neck cross section is nearly circular. Using only measurements of extremal areas, it would not be possible to distinguish, for example, between a circular and an elliptical cylinder. The magnetoacoustic method, giving direct dimensional measurements, is thus more adapted to detecting any possible asymmetry in the Fermi surface necks than the de Haas-van Alphen technique.

Table 1
Neck radii for the copper Fermi surface

Source of data	Neck Radii* ⟨110⟩	⟨112⟩
Present work - magnetoacoustic	0.925±.01	- -
Bohm and Esterling[13] "	0.96 ±.055	0.94±.055
Coleman and Funes[14] - magnetoresistance	0.91	0.82
Shoenberg[10] - de Haas-van Alphen	0.99)	) mean radii
Joseph, et al.[12] - "	0.930)	

*Dimensions in units of ka (see caption Fig. 10)

C. Thermal and Electrical Conductivity of High-Purity Rhenium Crystals from 2-20°K

The thermal conductivity of pure metals at low temperatures is due almost entirely to the conduction of heat by the electrons, since at these temperatures the lattice vibrations do not carry an appreciable amount of heat. The use of low temperature thermal conductivity to study electron motion in metals is limited by the fact that the electron scattering by impurities and defects increases as temperature decreases; indeed, impurity scattering becomes totally dominant as the limit, T=0°K, is approached. Most experimental thermal conductivity studies of pure metals have been such that the ideal thermal resistivity (i.e., the resistivity due to effects other than impurity scattering) have not been observable below 10° to 20°K.[15] Theoretical treatments of electron-lattice interactions have not yielded very satisfactory agreement with the data, and it has been suggested that experiments on highly perfect specimens, allowing comparisons between theory and experiment at lower temperatures, would yield better agreement between theory and experiment.[16] Very recently it has been proposed that electron-electron interactions can be much more important than electron-lattice interactions at very low temperatures in metals with complex Fermi surfaces.[17] In either case, the ideal thermal resistivity would vary linearly with the temperature, whereas the ideal thermal resistivity due to electron-lattice interactions is expected to vary as the square of the temperature.

Furthermore, the electron-electron theory predicts that the ideal electrical resistivity should vary as the square of the temperature and that the ideal Lorenz number, that is the ratio of the ideal electrical resistivity to the product of ideal thermal resistivity and temperature, would be temperature independent at the value of $1.08\times10^{-8} v^2/deg^2$. Data on one specimen of nickel are in good agreement with these predictions.[18]

In the present work a combination of highly sensitive measuring technique with single crystal specimens of very high purity have permitted the observation of the ideal thermal resistivity at temperatures from 20°K down to about 4°K. The specimens were prepared by electron beam zone-refining, and had electrical resistivity ratios between room and liquid helium temperatures of about 2500. One specimen, prepared by R. Soden of Bell Telephone Laboratories,[19] had a ratio of about 5000. The apparatus used in this work employed a Au-0.02%(at)Fe vs Ag-0.37%(at)Au thermocouples which were calibrated against the NBS 1965 Provisional Temperature Scale[20] via a germanium resistor, and has been described in detail elsewhere.

Both the thermal and electrical ideal resistivities observed in these experiments agreed, in the neighborhood of 20°K, with earlier measurements on less pure specimens. In the low temperature limit, however, the ideal electrical resistivity varied as T^2 and the ideal thermal resistivity varied as T, in agreement with the electron-electron interaction theory. The data for the most pure specimens, shown in Fig. 11, clearly indicate this behavior. The other specimens exhibited the same dependence on temperature, although the data showed somewhat more scatter. As can be seen in Fig. 12, the ideal Lorenz numbers are independent of temperature below about 11°K, in good agreement with the electron-electron interaction theory, although the actual value of $\sim 0.5\times10^{-8} v^2/deg^2$ differs from the theoretical value of $1.08\times10^{-8} v^2/deg^2$.

REFERENCES

[1] K.A. Jackson, Liquid Metals and Solidification, p. 174-186, A.S.M., Cleveland, Ohio, 1958.

[2] J.J. Kramer and W.A. Tiller, J. Chem. Phys. 37, 841 (1962).

[3] R.J. Schaefer and M.E. Glicksman, Rept. of NRL Prog., March 1967, p. 25.

[4] M.E. Glicksman and R.J. Schaefer, ARPA Annual Report (1966), Order No. 418, p. 58.

[5] K.A. Jackson and J.D. Hunt, Acta Met. 13, 1212 (1965).

[6] S. Doniach and S. Engelsberg, Phys. Rev. Letters 17, 750 (1966).

[7] N.F. Berk and J.R. Schrieffer, 10th Int. Low Temp. Conf., Moscow (1966).

[8] M. Rice, International Congress on Magnetism, Boston, Mass., 10-16 September 1967.

[9] D. Shaltiel, J.H. Wernick, and H.J. Williams, Phys. Rev. 135, 1346 (1964).

[10] Shoenberg, Phil. Trans. Roy. Soc. London, A255, 85 (1962).

[11] D.J. Roaf, Phil. Trans. Roy. Soc. London, A255, 135 (1962).

[12] A.S. Joseph, A.C. Thorsen, E. Gertner and L.E. Valby, Phys. Rev. 148, 569 (1966).

[13] H.V. Bohm and V.J. Easterling, Phys. Rev. 128, 1021 (1962).

[14] A.J. Funes and R.V. Coleman, Phys. Rev. 131, 2084 (1963).

[15] G.K. White and S.B. Woods, Phil. Trans. Roy. Soc. A251, 273 (1959).

[16] K. Mendelssohn and H.M. Rosenberg, Solid State Physics, Vol. 12, p. 240, Academic Press, New York (1961).

[17] C. Herring, Phys. Rev. Letters 19, 167 (1967).

[18] G.K. White and R.J. Tainsh, Phys. Rev. Letters 19, 165 (1967).

[19] R.R. Soden, G.F. Brennert, and E. Boehler, J. Electrochemical Soc. 112, 77 (1965).

[20] H. Plumb and G. Cataland, Metrologia 2, 127 (1966).

Fig. 1a - Influence of a grain boundary at a solid/liquid interface. The liquid phase is identified with the dark area.

Fig. 1b - Influence of a grain boundary at a solid/liquid interface. The liquid phase is identified with the dark area. Fig. 1b was taken approximately 30 seconds after 1a.

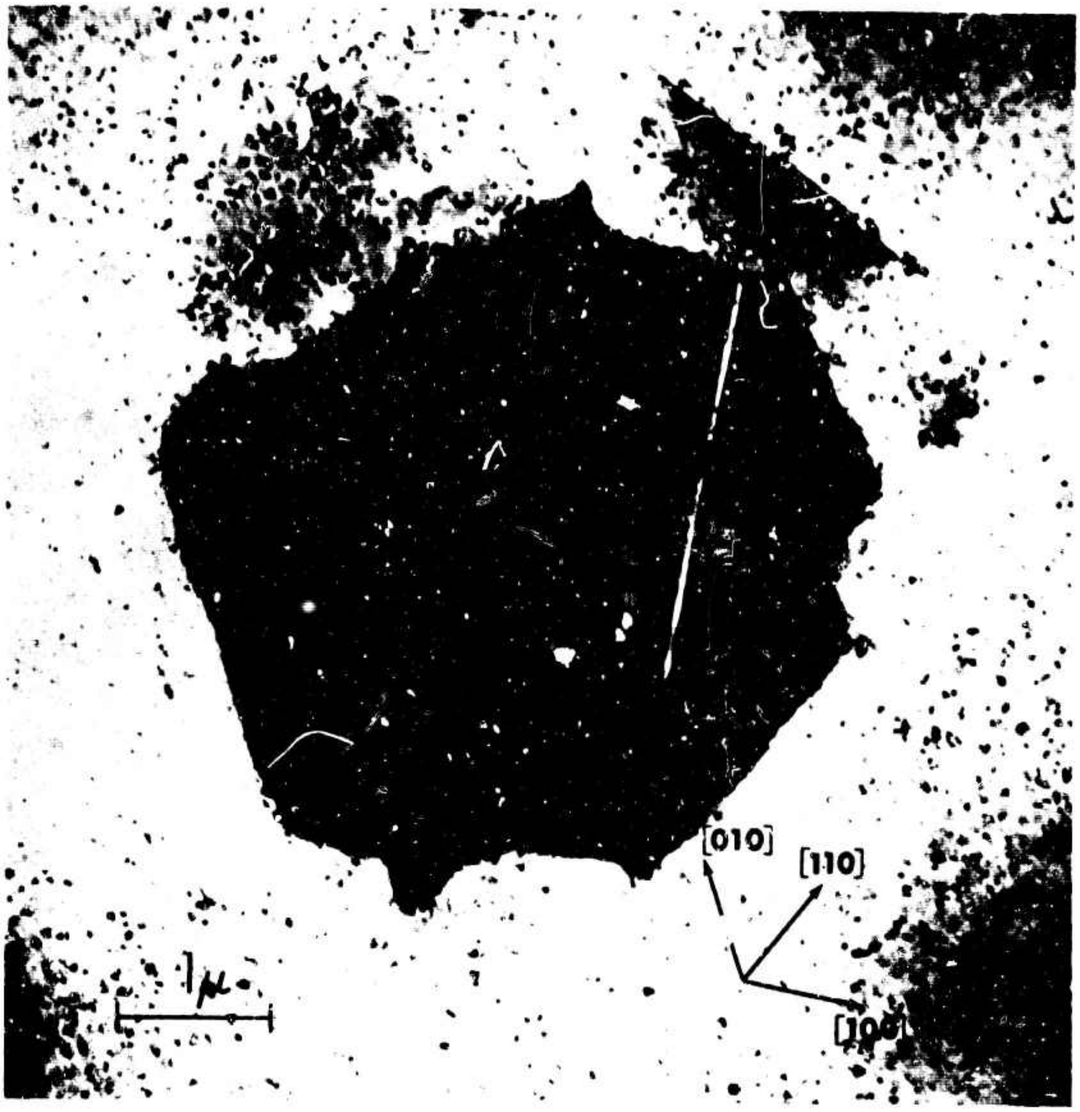

Fig. 2 - A "pool" of liquid within a large single crystal area

Fig. 3 - Liquid protruding into the single crystal

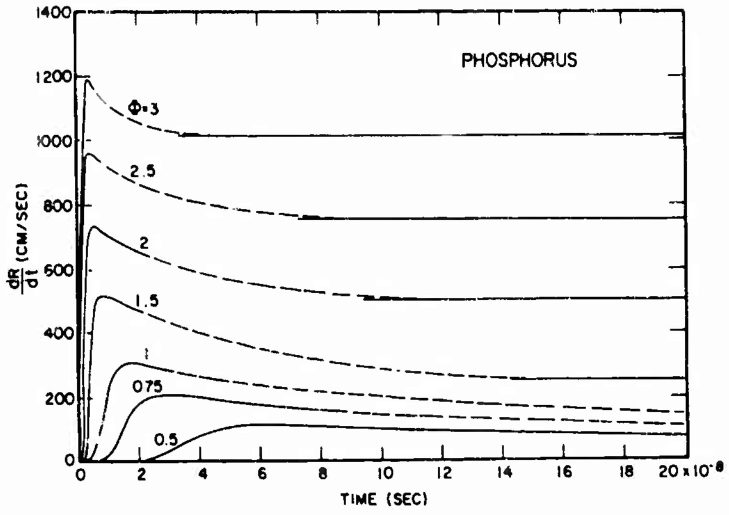

Fig. 4 - Growth rate of spherical nuclei in supercooled liquid phosphorus, for several values of the supercooling Φ. The solid lines represent computer-generated solutions during the initial stages of growth, and analytical solutions for the steady state growth rates. The dashed lines represent estimated behavior during the approach to steady state.

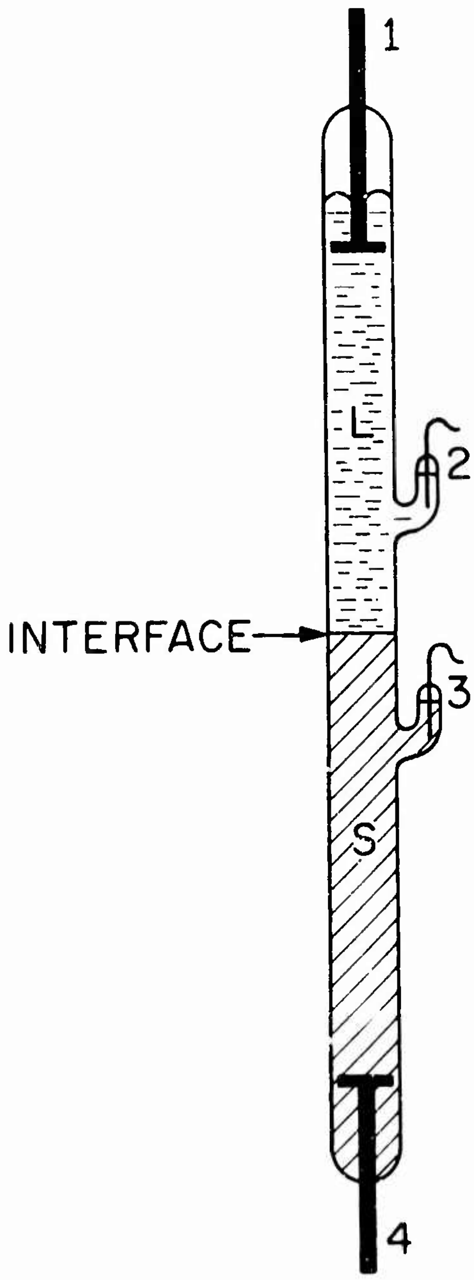

Fig. 5 - Apparatus for measurement of solidification kinetics. The square-wave current generating the Peltier heating and cooling is introduced through electrodes 1 and 4, whereas electrodes 2 and 3 are used in the electronic measurement of interface motion.

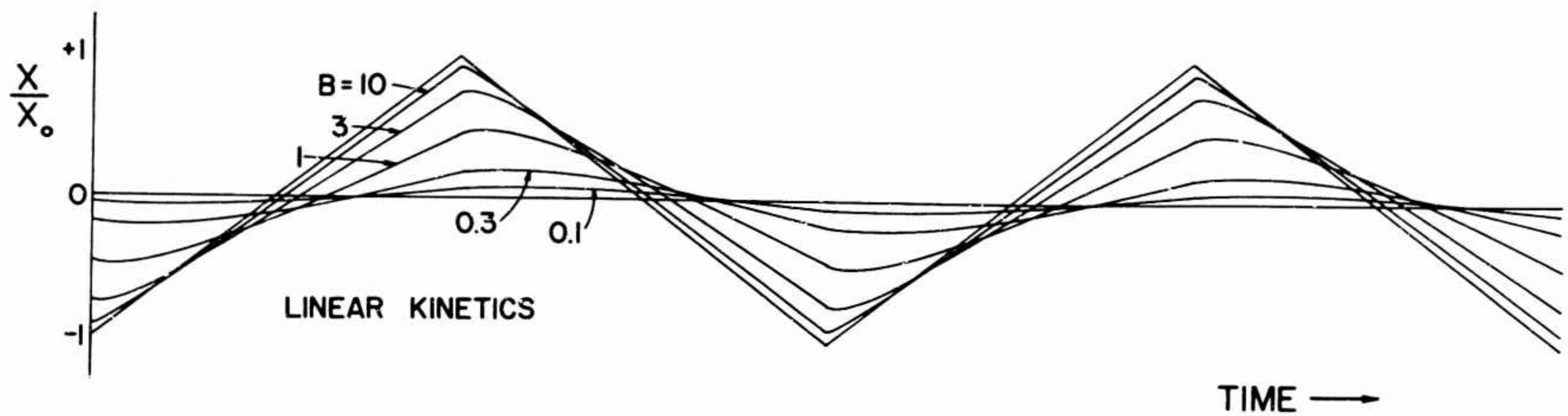

Fig. 6a - Response of interfaces to square-wave Peltier heating and cooling. Normalized displacement curves for interfaces with linear kinetics, $v = \mu \Delta T$. The parameter B is proportional to μ and inversely proportional to the square root of the fundamental frequency of the square wave.

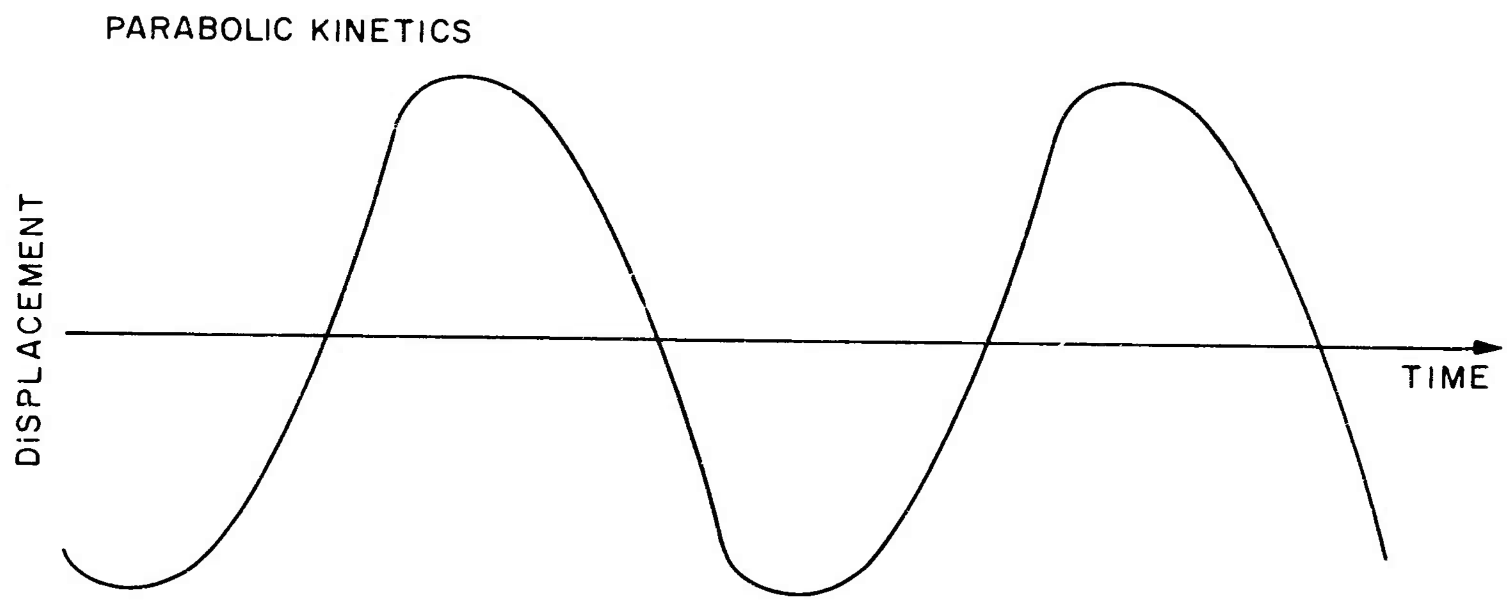

Fig. 6b - Response of interfaces to square-wave Peltier heating and cooling. Displacement of interface obeying the parabolic kinetic law $v = 3(\Delta T)^2$, subjected to 40 Hz square wave.

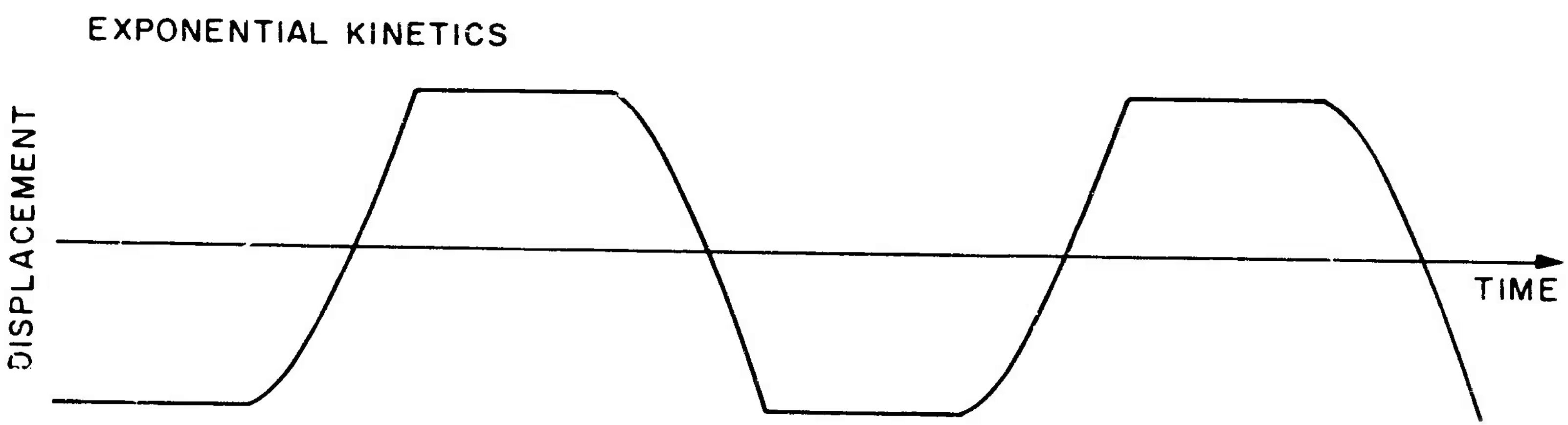

Fig. 6c - Response of interface to square-wave Peltier heating and cooling. Displacement of interface obeying the expotential kinetic law $v = 1.4 \times 10^{19} \exp(-50/\Delta T)$, subjected to 0.6 Hz square wave.

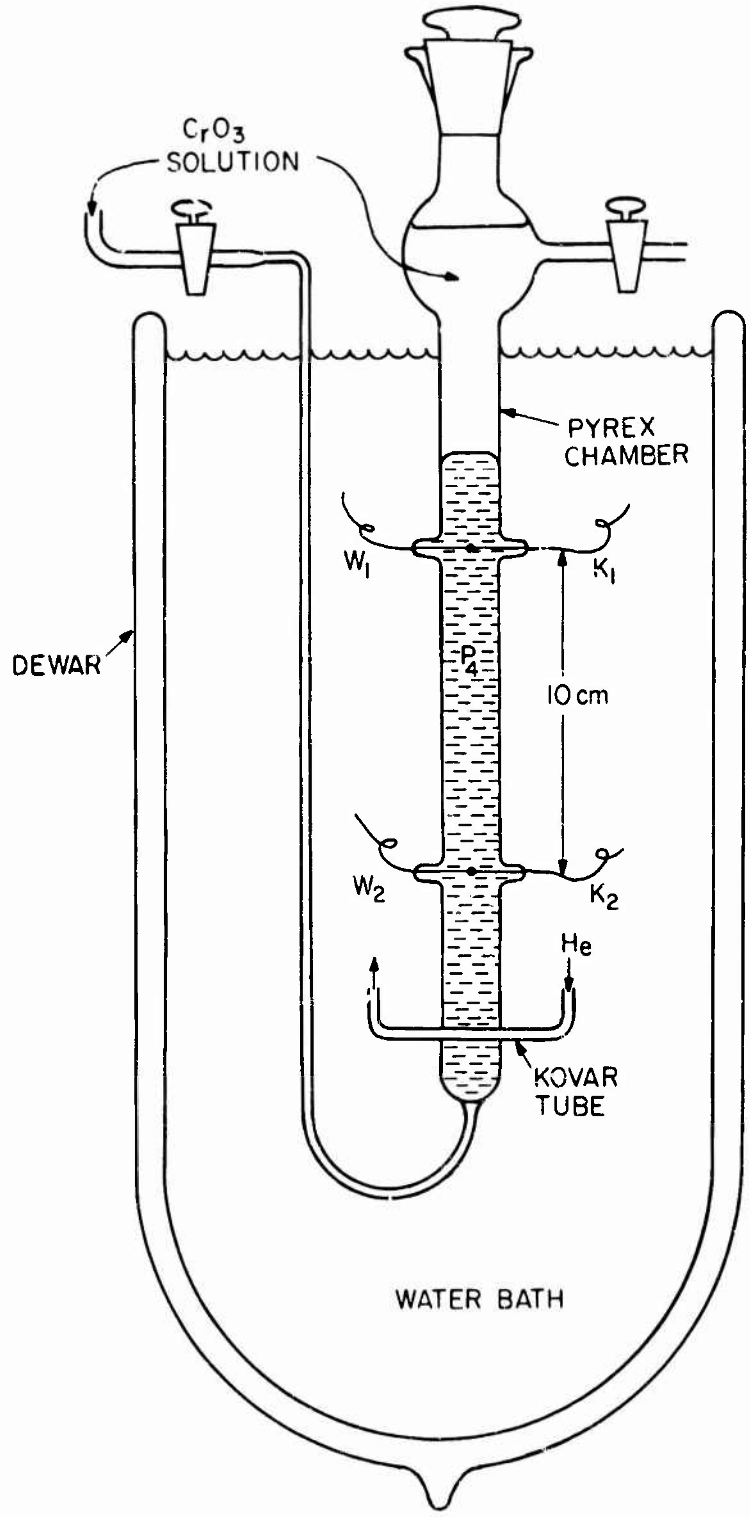

Fig. 7 - Apparatus for measuring solidification velocity in supercooled phosphorus, showing tungsten-Kovar-A thermocouples, helium-chilled triggering device, and flushing system

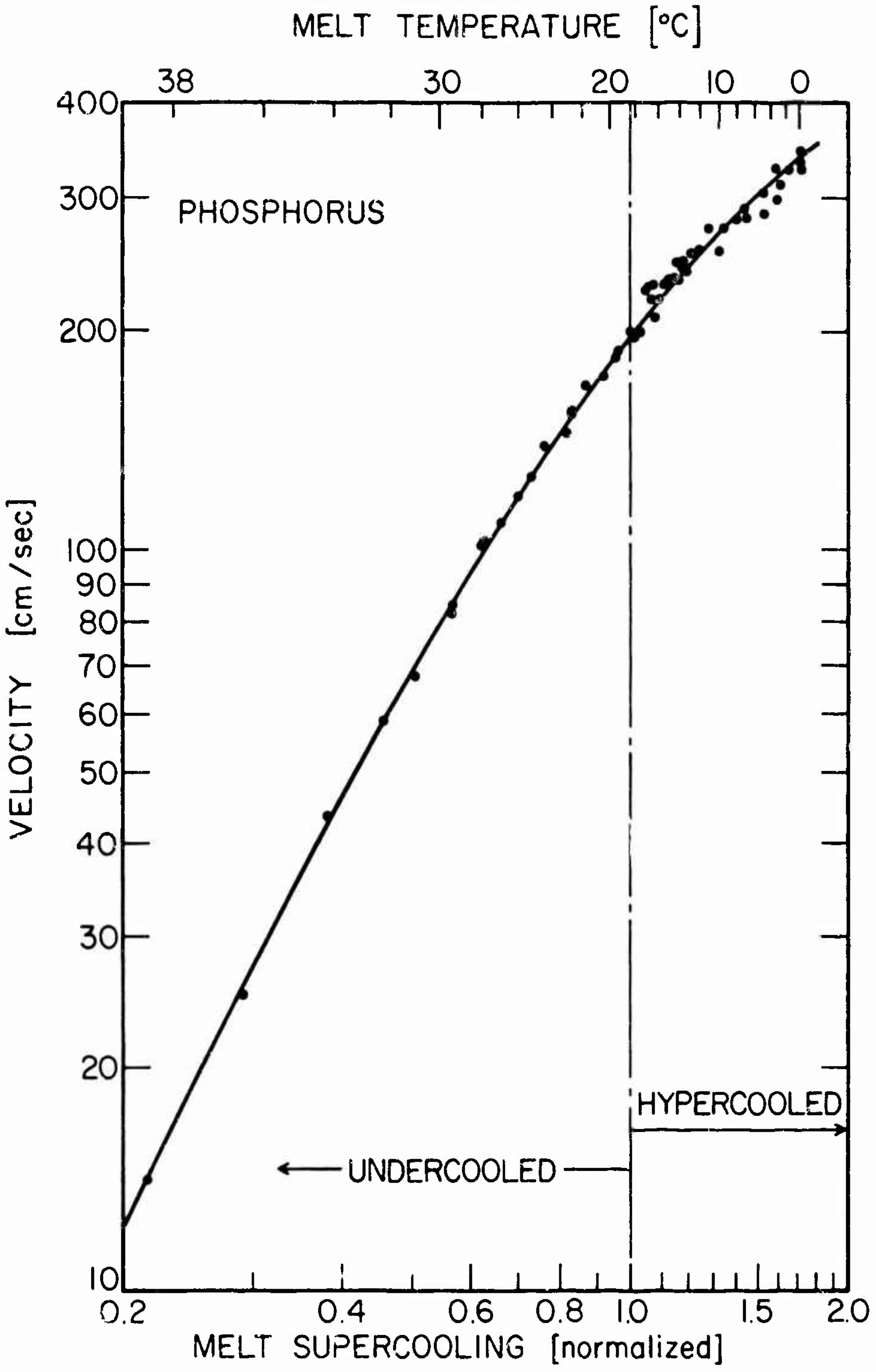

Fig. 8 - Solidification velocity as a function of melt supercooling (lower abscissa) and melt temperature (upper abscissa). ΔT_b^*, the minimum bath supercooling for total solidification, is unity on the lower (normalized) abscissa, where supercooling is given in units of λ / C_p^{ℓ}.

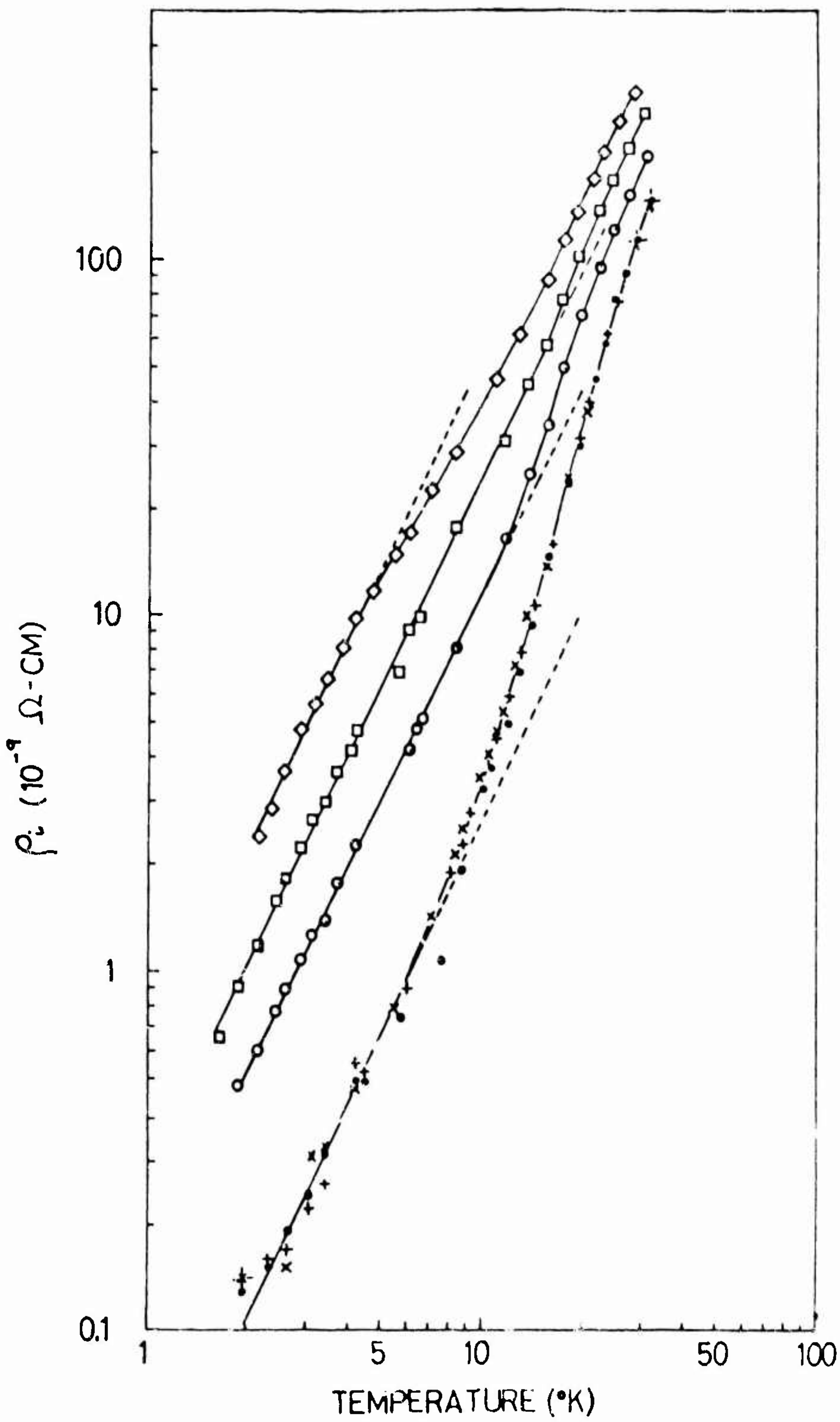

Fig. 9 - The ideal electrical resistivity as a function of temperature●+x, three high purity samples of pure palladium; o, Pd-1/2%Ni; □, Pd-1%Ni; ◇, Pd-1.66%Ni.

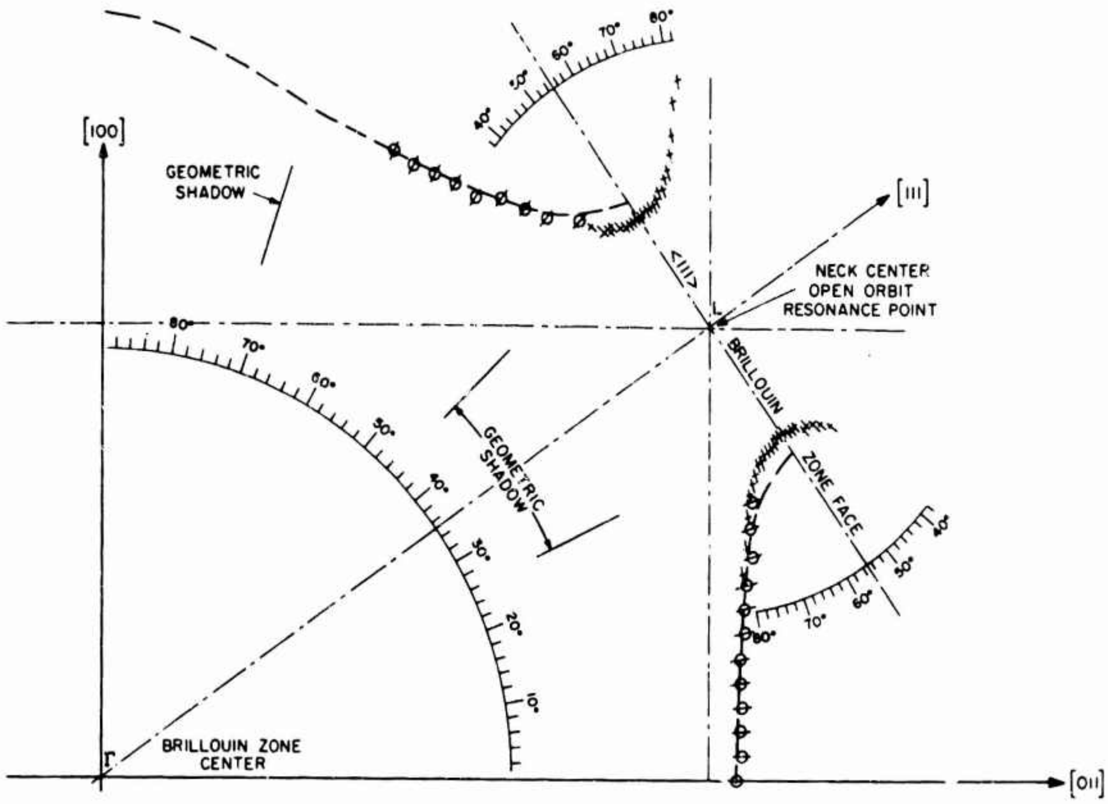

Fig. 10 - Magnetoacoustic measurements of the Fermi surface of copper in the (011) plane. Dimensions derived from oscillations attributed to neck orbits are indicated by crosses and are plotted from the neck center (point L of the Brillouin zone). Those dimensions derived from oscillations attributed to belly orbits are indicated by circles and are plotted from the zone center (point Γ). The angular ranges are indicated where the belly orbits are blocked by necks. The scales are in dimensionless units of ka, where k is the Fermi surface dimension in terms of cm^{-1} and a is the copper lattice constant at 4.2°K taken as 3.603×10^{-8} cm.

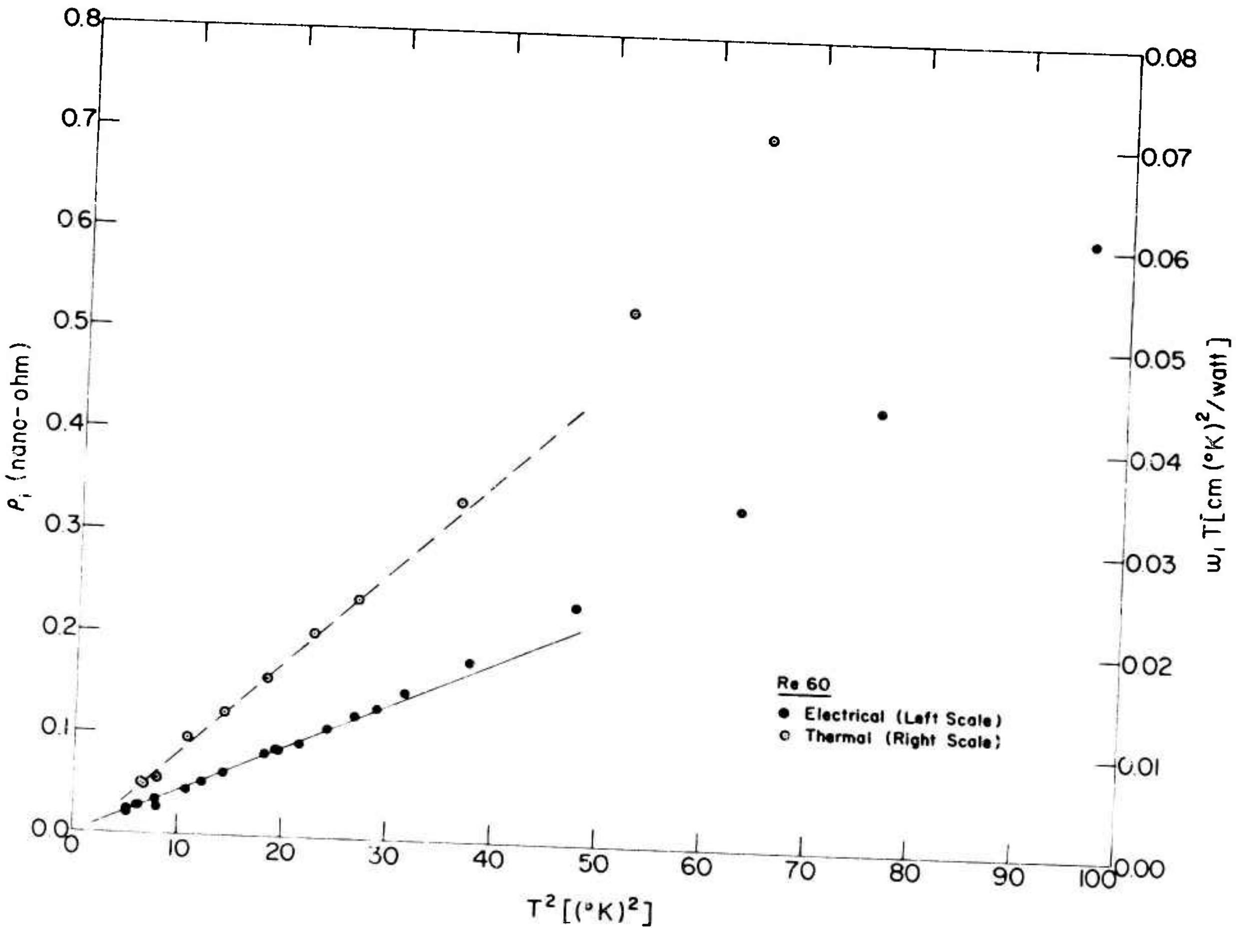

Fig. 11 - Ideal electrical resistivity (solid circles) and product of temperature and ideal thermal resistivity (open circles) as functions of the square of the temperature for rhenium specimen Re 60. The dashed and solid lines are simply straight lines drawn through the low temperature values where the data are apparently following $\rho_i \sim T^2$ and $w_i \sim T$.

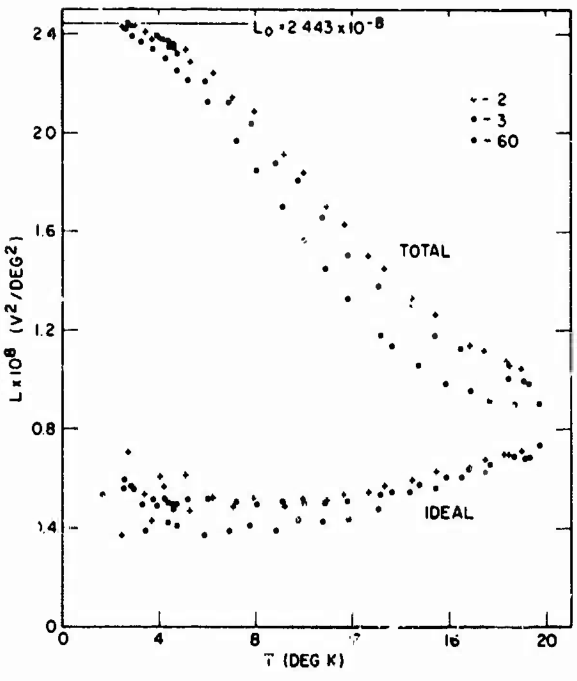

Fig. 12 - Temperature dependence of the Lorenz numbers of three rhenium specimens. The "total" curves were derived from the data in the usual way, while the "ideal" curves were obtained by using the ideal components of the resistivities.

MAGNETIC MATERIALS

Personnel Engaged in Program

Principal Investigator: G. T. Rado
V. J. Folen
W. G. Maisch
J. J. Krebs
R. A. Becker

INTRODUCTION

The main objectives of this program are the growth of single crystals containing transition metal ions, and the characterization of these crystals by magnetic and optical methods. An important adjunct to these experiments is the identification of the crystals by x-ray or other techniques. Phenomena associated with ordering in concentrated crystals, as well as interactions between ions in magnetically dilute crystals, are being studied. When appropriate, each material is studied by a variety of techniques in order to obtain the detailed characterization necessary for the understanding of the behavior of the material and for its evaluation for possible applications. It has been found necessary to grow these crystals in the Magnetism Branch since they are either unavailable elsewhere or cannot be obtained with the required characteristics. This report covers the period from 1 July 1966 to 30 June 1967.

CRYSTAL SYNTHESIS

A_2BF_4

The initial methods used in the present project for the synthesis of A_2BF_4 single crystals were discussed in the previous annual report. (In these crystals, A is an alkali metal ion and B is a divalent transition metal ion.) Some of these preparation methods yielded single crystals of K_2CoF_4 and K_2ZnF_4, the latter being doped with Mn^{2+}, Fe^{3+} or Co^{2+}. It has since been determined that, in order to prepare other crystals of this type, more elaborate tehhniques will be required. Specifically, (1) the starting materials (fluorides) are unstable and must be purified, i.e., hydrates, oxides, and basic salts must be converted back to the fluoride; and (2) the purified reactants must be protected from oxidation during crystal growth.

In order to reduce the oxidation problem a vacuum single crystal furnace was constructed for the preparation of some of these fluoride materials. In addition, the construction of apparatus for the purification of the starting materials is now partially completed. In this apparatus, the impure chemicals are heated in a HF atmosphere so that corrosion resistant components must be utilized. These include an inconel reaction tube, monel valves, teflon gaskets and teflon or copper tubing.

$Al_2O_3:Fe^{3+}$

Single crystals of α-Al_2O_3 doped with Fe^{3+} have been grown with nominal Fe^{3+}/Al^{3+} ratios of 0.001, 0.002, 0.005, 0.01 and 0.02.

CRYSTAL CHARACTERIZATION

K_2CoF_4

K_2CoF_4 crystals are tetragonal (space group D_{4h}^{17} , a = 4.07 A, c = 13.08 A) with two molecules per unit cell. One Co^{2+} ion is located at 0,0,0 and surrounded by six F^- ions at (± 1/2, 0,0), (0, ± 1/2,0), and (0,0 ± Z) (Z $\approx$ 1/2 a), while the second $(Co\ F_6)^{-4}$ octahedron is displaced by (1/2, 1/2, 1/2). The F^- ions at (± 1/2, 0,0) and (0, ± 1/2,0) (and the equivalent set displaced by (1/2, 1/2, 1/2)) are shared by neighboring octahedra, while the other F^- ions are not. The crystal, then, can be considered to be made up of layers of octahedra separated by c/2, with adjacent layers displaced by $\sqrt{2}/2$ a along the [110] direction. Two K^+ ions are symmetrically located between each pair of octahedra along the c axis. The crystal is paramagnetic at high temperatures and becomes antiferromagnetically ordered below 145°K. Of primary interest is the fact that the ordering is two dimensional, occurring within each 001 plane. As will be seen below, the optical properties of the crystal are also anisotropic.

The optical absorption spectrum of single crystals of K_2CoF_4 was observed in σ, π, and axial polarizations in the region 5000-50,000 cm^{-1} at ten different temperatures between 4.2°K and 300°K. Two narrow regions of the spectrum (near 7000 cm^{-1} and 23,000 cm^{-1}), in which sharp bands appeared at 77°K and below, were scanned at three additional temperatures.

The gross features of these spectra have been identified with transitions of the $3d^7 Co^{2+}$ ion in a cubic crystalline field. The effect of the axial field, although evident in the room-temperature spectra, are best seen at 4.2°K. At this temperature, the sharp bands which appear on the low frequency side of the $^4T_{1g} \rightarrow {}^4T_{2g}$ band at 77°K and below are located at 6917 and 6984 cm^{-1} in the σ spectrum and at 69[illegible]3 and 699[illegible] cm^{-1} in the α and π spectra. The location and intensities of these bands in the three spectra show that they are pure magnetic dipole transitions. Similar information for the broad $^4T_{1g} \rightarrow {}^4T_{2g}$ transition indicates that it is at least partially magnetic dipole in character. The four bands betwen 17,000 mm^{-1} and 22,000 cm^{-1} (transitions from the $^4T_{1g}$ ground state to $^2T_{1g}$, $^2T_{2g}$, $^4T_{1g}$, and $^2T_{1g}$) are split into a number of partially resolved components. A comparison of the σ, π and axial spectra shows that each band has both electric dipole and magnetic dipole components. In addition, very weak bands near 23,000, 26,700 and 28,[illegible] cm^{-1} appear to be highly polarized.

As was indicated above, the absorption bands become narrower and more highly resolved as the temperature is lowered. There is also a large reduction of intensity on the low-frequency side of the $^4T_{1g} \rightarrow {^4T_{2g}}$ and $^4T_{1g} \rightarrow {^4T_{1g}}$ bands, resulting from the depopulation of the low-lying vibrational and spin-orbit levels of the ground $^4T_{1g}$ state. Finally, sharp bands near 7000 and 23,000 cm^{-1} appear at 77°K and below. As the temperature is lowered, these bands become narrower and the absorption peak of each band becomes more intense and shifts to higher frequency. Unfortunately, thermal interactions cause these bands to disappear above 77°K, so that the effect of magnetic ordering (T_N = 145°K) on the bands cannot be observed.

$K_2ZnF_4:Mn^{2+}$

Electron spin resonance (ESR) measurements at 24 KMc have been made on single crystals of K_2ZnF_4 doped with Mn^{2+}. The angular dependence of the ESR spectra in these measurements was found to be consistent with 4-fold axial symmetry about the crystallographic c-axis. These measurements yielded values of the spin Hamiltonian parameters, $g_{\parallel}$, $g_{\perp}$, D, A, B, a and F. In addition, the superhyperfine structure (which results from an interaction of the fluorine nuclei with the 3d electrons in Mn^{2+}) showed that the Mn^{2+} ions do indeed reside in the Zn^{2+} sites. From measurements with the applied magnetic field (H) in the [110], [100] and [001] crystallographic directions, the superhyperfine parameters A_s^{I}, A_s^{II}, A_p^{I} and A_p^{II} were evaluated. Here A_s describes the contact interactions at the F^- nuclei resulting from the bonding of the Mn^{2+} 3d electron orbitals with the F^-2s orbitals and A_p denotes $A_D + A_\sigma - A_\pi$, where A_D is the magnetic dipole - dipole interaction between the F^-

nucleus and the moment on the Mn^{2+} ion and A_σ and A_π represent, respectively, the Mn^{2+} 3d bonding interactions with the F^- 2 p_σ and F^- 2 p_π orbitals. The superscript I represents the 4 equivalent nearest neighbor F^- ions in the (001) plane and the superscript II represents the 2 equivalent nearest neighbor F^- ions along the four-fold axis in K_2ZnF_4. As deduced from the measured A - values, the unpaired spin densities in the fluorine 2s orbitals were found to be 0.6% for each type I and 0.4% for each type II fluorines. In order to obtain accurate values for the superhyperfine parameters, it was necessary to exactly diagonalize the appropriate interaction Hamiltonian because the F^- nuclear moments are not in general aligned parallel to H on account of the anisotropy in the superhyperfine interaction tensor.

$K_2ZnF_4:Fe^{3+}$

Room temperature ESR measurements of the spin-Hamiltonian parameters and the superhyperfine parameters in iron-doped K_2ZnF_4 at 24 KMC are partially complete. The spectra studied in these measurements correspond to Fe^{3+} in the Zn^{2+} sites. Preliminary values of the spin-Hamiltonian parameters (D, A, F and g) and the superhyperfine parameters have been determined from measurements with H in the [001], [110] and [100] directions. It appears that non-local charge compensation occurs for Fe^{3+} in the divalent site so that the Zn^{2+} site symmetry is preserved.

$Al_2O_3:Fe^{3+}$

The optical spectrum of the series of Fe^{3+} doped α-Al_2O_3 crystals mentioned above has been examined in the region 0.3 - 1.5 μ. Measurements were taken in the σ, π and axial polarizations and at temperatures of ~ 20°K, 77°K and 300°K. There is a considerable improvement in the resolution of the spectrum at liquid nitrogen temperatures. The major sharp features of the spectra are reasonably well explained by the effect of a cubic crystal field on the Fe^{3+} energy levels. However, the presence of an additional spectrum not attributible to Fe^{3+} has made it impossible to observe the important long wavelength components of the Fe^{3+} spectrum. X-ray fluorescence analysis of some of the crystal has shown that the actual iron concentration is close to the nominal value. The ESR spectrum of the crystals has also been examined with special emphasis on the existance of exchange coupled Fe^{3+} ion pairs. Such pair lines have been seen at room temperature and at microwave frequencies of 9.4, 24.0 and 34.8 GHz. Their identity has been established by means of their intensity relative to the single ion lines.

FUTURE PROGRAM

Attempts will be made to synthesize single crystals of K_2MnF_4, $NaMnF_3$ and other similar compounds. Optical studies are being planned for other crystals of the type A_2BF_4, including diamagnetic crystals doped with transition metal ions. Other experimental methods, such as luminescence studies, will be used to obtain additional information about the energy levels in these crystals.

The ESR measurements on K_2ZnF_4 doped with Fe^{3+} will be continued by measurements on additional single crystals and at low temperatures.

Oxidation and reduction experiments are planned to try to get rid of the objectionable non-Fe^{3+} optical spectra in Fe^{3+} doped Al_2O_3. The Fe^{3+} spectra will be analyzed in terms of crystal field theory. More work on the ESR spectrum of exchange-coupled Fe^{3+} pairs is planned especially in the liquid helium temperature range.

REFRACTORY METAL CRYSTALS

Personnel Engaged in Program

Principal Investigator: M. R. Achter

T. C. Reuther, Jr.
R. G. Vardiman
C. L. Vold*
T. G. Digges, Jr.†
1 Technician

*Part-time
†Now graduate student, Lehigh University

REFRACTORY METAL CRYSTALS

BACKGROUND

The long term objective of this program was the preparation and study of highly perfect specimens of refractory metals in which the only structural feature was a grain boundary of controlled misorientation. To achieve this purpose it was necessary to develop techniques for the production of highly perfect single crystals and for joining them to make bicrystals of controlled misorientation. The accomplishments of this program in five areas listed below are summarized:

1. Growth of single crystals of niobium.
2. Characterization of single crystals by x-ray techniques.
3. Optical observation of dislocation structures.
4. Sintering of intergranular porosity.
5. Grain boundary self diffusion in bicrystals.

1. GROWTH OF SINGLE CRYSTALS OF NIOBIUM

It was decided to grow the crystals by the strain anneal technique since it has been reported that they are more perfect than those grown from the melt. The growth of niobium crystals up to one inch in diameter, which are twice the size of the largest refractory metal crystal previously reported, were described in a technical note.(A)

2. CHARACTERIZATION OF SINGLE CRYSTALS OF NIOBIUM BY X-RAY TECHNIQUES

Dislocation densities were determined by means of double crystal spectrometer measurements and subgrain boundary tilt angles were measured by means of x-ray metallographic techniques. The variations of these parameters with processing variables were discussed in a published paper in terms of dislocation theory.(B)

3. OBSERVATION OF DISLOCATIONS BY OPTICAL MICROSCOPY

In the bicrystal sintering work described in Section 4, it was found necessary to have a detailed knowledge of the dislocation structure. Two methods have been commonly used to observe the dislocation line structure in metals. In transmission microscopy, besides the drawback of difficult specimen preparation, a lower limit of about $10^8 cm^{-2}$ exists for the dislocation density. X-ray micrography, on the other hand, has an upper limit of about $10^5 cm^{-2}$ for the density in a material like niobium. Since the dislocation densities of interest in niobium single and bicrystals lie precisely in this 10^5-$10^8 cm^{-2}$ range, different techniques are required.

Two methods for dislocation observation in niobium have been developed in this study. For easily obtained information on dislocation density and arrangement, etch pits at surface intersection sites are adequate. An electroetching technique has been investigated and perfected for this purpose. For more detailed observation of the dislocation line structure, a decoration and chemical etch technique has been found to give excellent results. A paper describing these techniques and giving some results obtained by them, has been submitted for publication. (C)

Electroetching

An electrolyte of H_2SO_4 + 10-15% HF serves for both electropolishing and electroetching. Pits in the shape of equilateral triangles have been found on {111} surfaces. By etching the curved sides of rods of various orientations, it has been determined that triangular pits may be developed at all orientations between the {111} pole and planes of the <111> zone. The pit shapes vary in a manner consistent with the development of {110} planes as the initial pit sides. This would of course be impossible beyond the <111> zone planes.

As-grown crystals sometimes show incomplete pitting, and fresh dislocations cannot be pitted in untreated material. It has been found that the addition of a s all amount of carbon allows the pitting all dislocations. This is illustrated in Fig..3-1. The carbon is evaporated on to the surface and diffused in at 1050°C. The increase of carbon content near the surface is less than 10 ppm. In contrast, large additions of nitrogen and of oxygen had no effect.

Electroetching effects, such as conical pits or film formation, have been observed at other orientations, but these proved either unreliable or inferior to the method described in the next section.

Chemical Etching

On surfaces which have been heavily doped with carbon, so that carbon concentration to a depth of about 200 microns is in the range of 50-60 ppm, an etch with nitric acid plus 15-30% hydrofluoric acid (which normally acts as a chemical polish) has been found to bring out the complete dislocation line structure of a surface layer. This effect is independent of surface orientation. Examples of the dislocation structure developed in strain anneal grown crystals are given in the figures below.

The dislocations etch more slowly than the surrounding area and so become raised above the surface. The resolution is approximately the width of the affected region around the dislocation, which is of the order of one half micron. The sharpest relief is found for the most freshly etched part of the dislocation line. As the surface is etched below the original position of the line, the "hill" begins to polish out, gradually fading away. The disappearance of a particular segment of dislocation line may require the removal of up to 30 microns of material, and so the thickness of the layer from which dislocations are visible increases with etching time up to this value. The process is illustrated in Fig. 3-2 in which two stages of etching of a double helix are shown. The helical axis is a <111> direction lying at 19.5° to the surface. Two views from Fig. 3-2a are drawn in Fig. 3-3, showing that the layer in this case is 14 microns deep. After further etching, in Fig. 3-2b, it has increased to slightly over 30 microns.

In general a dislocation in a subgrain interior will show two endpoints. One of these will be faded, representing the first appearance of a dislocation on etching. The other will be sharp corresponding with the intersection of the dislocation with the actual surface. In determining the dislocation density, these latter points are counted, in the same manner as etch pits, and the formula $n = 2\rho$ applied. n is the dislocation density in cm. per cm.^{3}, and ρ the density of intersection points by chemical etching or of pits by electroetching. Densities obtained by the two methods agree closely, and their equivalence is shown in Fig. 3-4. Here a chemically etched {111} surface was subsequently electroetched. Although some detail in the raised structure has been lost during the electroetch, it can be seen that all raised dislocations terminate in etch pits.

The structure of subboundaries lying at relatively small angles to the surface may be resolved for misorientations up to at least one minute corresponding to a dislocation spacing of one micron. The net shown in Fig. 3-5 is close to the configuration for a pure twist boundary, with a prominent <100> component. Such pure twist boundaries limited to {110} surfaces in b.c.c. structures, were rarely observed. A pure tilt boundary on a {111} surface is shown in Fig. 3-6. In this case a <110> dislocation line direction probably corresponds to a {211} slip plane perpendicular to the surface.

Boundaries which lie at greater angles to the surface may still be resolved if the misorientation is not too great. However, many subboundaries appear only as ridges of unresolvable structure, due to the density of dislocations in them, or the complexity of their structure.

4. SINTERING OF INTERGRANULAR POROSITY IN BICRYSTALS

Bicrystals of niobium are made from half-inch diameter single crystals which have been grown by the strain anneal method. Discs are cut, spark planed, and electro- or chemically polished. Symmetrical tilt boundaries are produced by rotating one disc by 180° with respect to another cut from the same crystal, and pressure welding in a vacuum induction heating furnace at 1500°C. The bicrystal is then sectioned longitudinally, electropolished, lightly etched and the void density counted. Suitable correction is made for the enlargement of the voids on etching.

Annealing behavior at 1800°C for a zero angle and a high angle tilt boundary is shown in Fig. 4-1*. Both boundaries show a similar large decrease in sintering rate with annealing time. The likliest explanation for this behavior is that dislocations which are introduced during welding act as vacancy sinks to produce an initial high sintering rate. The rate decreases as the dislocation density decreases during the anneal. This explanation is supported by the behavior of bicrystals welded at different pressures, as shown in Fig. 4-2. The large difference in the curves for 250 and 300 psi is presumably due to the fact

*Note that in Section 5 a sintering temperature of 2200°C is used to eliminate porosity completely.

that the yield strength for this material at 1500°C lies in this range. The large change in dislocation density and arrangement after a one hour anneal at 1800°C for a 300 psi specimen is shown in Fig. 4-3. The decoration and chemical etch technique described in Section 3 has been used here to bring out the dislocation structure. Present work is directed toward correlating the sintering rate with dislocation density.

5. GRAIN BOUNDARY SELF DIFFUSION IN BICRYSTALS OF NIOBIUM

Introduction

Grain boundary self diffusion is being studied in bicrystals of controlled crystal and boundary orientation which are prepared by sintering together single crystal discs.* The diffusional penetration of niobium-95 tracer into synthetic grain boundaries is studied as a function of orientation with the object of providing insight into the structure of the boundaries.

The grain boundary diffusion model of Fisher(1), Fig. 5-1, in which the diffusant penetrates a semi-infinite isotropic medium of constant diffusivity, D, that contains a slab of thickness δ and diffusivity D' (>>D) is used. In the present experiments the exact solution of Whipple(2) and the complementary and interpretative numerical computation of LeClair(3) was applied to this model in order to interpretate and assess the data.

For a sintering experiment, LeClair presents the applicable solution in the form

[1] $$D'\delta = \left(\frac{\partial \ln \bar{c}}{\partial y}\right)^{-2} \left(\frac{4D}{t}\right)^{1/2} \left(\frac{\partial \ln c}{\partial (\eta\beta^{-1/2})}\right)^{2}$$

where t is the time of diffusion, $\bar{c}$ is the average concentration (or activity) in a semi-infinite layer of thickness dy, and where η and β are the reduced and dimensionless

*See Section 4 for details of preparation.

parameters of Whipple,

$$\eta = y/(Dt)^{1/2}$$

and

$$\beta = \frac{D'}{D} \frac{1/2\ \delta}{(Dt)^{1/2}}$$

The computation of LeClair(3), in accord with the insight of Levine and MacCollum(4) and Suzuoka(5) reveal that Eq. 1 is more readily evaluated if it is transformed to

$$[2] \qquad D'\delta = \left(\frac{\partial \ln \bar{c}}{\partial y^{6/5}}\right)^{-5/3} \left(\frac{4D}{t}\right)^{1/2} \left(\frac{\partial \ln \bar{c}}{\partial(\eta\beta^{-1/2})^{6/5}}\right)^{5/3}$$

For [2], the final term is nearly constant in $\eta\beta^{-1/2}$ and for $\beta>$ about 5, this is

$$\frac{\partial \ln \bar{c}}{\partial(\eta\beta^{-1/2})^{6/5}} = 0.78$$

In practice then, a plot of $\ln \bar{c}$ vs (penetration distance)$^{6/5}$ should be a straight line at depths where lattice diffusion does not contribute and from the slope of such a plot, $\partial \ln \bar{c}/\partial y^{6/5}$ is obtained. The second term is evaluated for the diffusion time, t, and the known (at a given temperature) value of D from lattice diffusion measurements.

Experimental Procedure

Bicrystals that are produced by sintering at 2200°C are sectioned perpendicular to the grain boundary and electropolished. Niobium-95 tracer then is vacuum evaporated onto the electropolished surface.* Diffusion anneals are done in vacuum ($<2\times10^{-6}$) and temperature is controlled to $\pm$ 1°C and at time and temperature that limit lattice penetration ($\approx\sqrt{4Dt}$) to about 2×10^{-6}cm. The concentration-penetration data are then obtained by serially sectioning the bicrystal in layers parallel to the tracer deposit and perpendicular to the grain boundary. The activity of each layer is then obtained by counting the 0.75 Mev γ-peak of Nb-95.

---

*Deposition Nb-95 was done through the courtesy of Metals and Ceramics Division of ORNL.

The key to this experiment is the sectioning technique. The process developed by Pawel and Lundy(6) in which the sample is sequentially anodized to a given voltage and then stripped of the dielectric, anodic film is used to obtain layers of 455A (±10%). [A calibration of voltage vs thickness was obtained by interferometric measurements and is in accord with the independent calibration of Lundy et al.(7).] The resolution of this sectioning technique allows concentration-penetration curves to be determined for total penetration distance of as little as 0.4 microns.

Bicrystals on which diffusion measurements have been or will be made are listed in Table I. As indicated in the table, most have symmetrical "tilt" boundaries with rotations, θ, about <100>, <111> or <110>, but several "random" orientations of unspecified but high index axes are also included. The angle ø is the deviation from the listed <h k l> rotation axis. All of the symmetrical bicrystals were sectioned normal to the tilt axis.

An example of the concentration-penetration data is presented in Fig. 5-2a. These data are first plotted as log activity vs (Penetration Distance)^2 which for lattice diffusion, should yield a straight line(8). Clearly the curvature indicates that enhancement is observed. In Fig. 5-2b, log activity (per layer) is plotted vs (penetration distance)$^{6/5}$ in accord with Eq. 2. A reasonable straight line is obtained at the deeper penetrations where lattice diffusion does not contribute. The count rate data are corrected for decay and background and the error flags indicate the sum of the statistical counting error (<2%) and the variation in background (~10± 1 cpm).

The value of D'δ is obtained from Eq. 2, and these results are given in Table 2 for the samples that have been completed. From the <100> and <111> crystals diffused at 1000°C for 6 hr. two points are evident: First, from the shape of the curves there is measured enhancement at the smallest misorientation and second, the degree of enhancement increases with increasing misorientation. While the former observation could be caused by another enhancement mechanism (eg., forest or subboundary dislocation pipe diffusion) the apparent orientation dependence could only come from a boundary effect.

The possibility of non-boundary enhancement is being checked experimentally by doing self-diffusion measurements on single crystals in both the virgin state and after handling that is identical to the bicrystal processing.

The temperature variation of $D'\delta$ was obtained for the random boundaries. A plot of log $D'\delta$ vs 1/t for the 950, 1000 and 1050°C anneals yield an activation energy of 51 k.cal./g atom/°K. The activation energy for lattic diffusion is 96 k.cal.(7).

In addition to $D'\delta$, the tabulated results include $D'\delta/D$, β and D'/D. From Suzuoka(5) and LeClair(3), the value of β is probably the best indicator of the validity of a grain boundary experiment. The values obtained in the present experiments are representative of those expected for a valid experiment in accord with the model and solution that have been used.

REFERENCES

1. J. C. Fisher, J. Appl. Phys. 22: 74 (1951).

2. R.T.P. Whipple, Phil. Mag. 45: 1225 (1954).

3. A. D. LeClair, Brit. J. Appl. Phys. 14: 351 (1963).

4. H. S. Levine and C. J. MacCallum, J. Appl. Phys. 31: 595 (1960).

5. Toshiro Suzuoka, J. Phys. Soc. Japan 19: 839 (1964).

6. R. E. Pawel and T. S. Lundy, J. Appl. Phys. 35: 435 (1964).

7. T. S. Lundy, F. R. Winslow, R. E. Pawel and C. H. McHargue, AIME Met. Soc. Trans. 233: 1533 (1965).

8. W. A. Johnson, Trans. AIME 143: 107 (1941).

6. PUBLICATIONS

A. T. G. Digges, Jr. and M. R. Achter, "Growing Large Single Crystals of Niobium by the Strain-Anneal Method", Trans. AIME 230 (1964) 1737.

B. M. R. Achter, C. L. Vold and T. G. Digges, Jr., "X-ray Diffraction Study of the Perfection of Niobium Single Crystals", Trans. AIME 236 (1966) 1597.

C. R. G. Vardiman and M. R. Achter, "Dislocation Structures in Niobium Single Crystals Observed by Optical Microscopy", submitted for publication.

TABLE 1

SINTERED BICRYSTALS FOR USE IN MEASURING GRAIN BOUNDARY SELF DIFFUSION IN NIOBIUM

Symmetrical Tilt Boundaries

<100> Axis of Rotation

No.	θ (deg)	φ (deg)
37A	2	2
34	5	2
39A	8	1
47	14-1/2	0
46A	20	2
38	20	1
61	22	0
36	23-1/2	1/2
60	26	0
44	28	0
52	39	0

<111> Axis of Rotation

No.	θ (deg)	φ (deg)
56	7	0
14	7	1/2
18	8	1/4
57	9	0
42	15	0
40	40	2
58	40	0

<110> Axis of Rotation

No.	θ (deg)	φ (deg)
59	15	0

"Random" Boundaries

No.	θ	φ	Axis <h k l>
17A	38	10	<100>
49A	8	18	<111>
50A	10	14	<111>
51A	42	28	<111>
53A	16	17	<110>

Note: θ is the amount of rotation about <h k l> axis and φ is deviation from the exact <h k l> indicated.

TABLE 2

RESULTS OF GRAIN BOUNDARY SELF DIFFUSION IN BICRYSTALS OF NIOBIUM

Symmetrical Tilt Boundaries (1000°C/6 hr)

Axis	θ	φ	D'δ (cm^3/sec)	D'δ/D (cm)	D'/D	β
<100>	2	2	$7.3x10^{-21}$	$1.6x10^{-4}$	$3.2x10^3$	78
"	8	1	$9.3x10^{-21}$	$2x10^{-4}$	$4x10^3$	99
"	20	2	$17.1x10^{-21}$	$3.7x10^{-4}$	$7.3x10^3$	183
<111>	7	1/2	$6.7x10^{-21}$	$1.5x10^{-4}$	$2.9x10^3$	72.5
"	8	1/4	$10.8x10^{-21}$	$2.3x10^{-4}$	$4.7x10^3$	116
"	40	2	$16.1x10^{-21}$	$3.5x10^{-4}$	$6.9x10^3$	172

Random Boundaries

Axis	θ	φ	D'δ (cm^3/sec)	D'δ/D (cm)	D'/D	β	Temp/time
<111>	42	28	$7.12x10^{-22}$	$6.8x10^{-5}$	$1.3x10^3$	34	950°C/27 hr
<110>	16	17	$1.8x10^{-21}$	$3.8x10^{-5}$	$7.7x10^2$	20	1000°C/6 hr
<111>	10	14	$3.4x10^{-21}$	$1.8x10^{-5}$	$3.5x10^2$	3	1050°C/1.5 hr
<100>	38	10	$3.6x10^{-19}$	$7.5x10^{-4}$	$1.5x10^4$	283	1075°C/1 hr
<111>	8	18	$3.1x10^{-19}$	$6.5x10^{-4}$	$1.3x10^4$	247	1075°C/1 hr

Note: The orientation variables have the same meaning as in Table 1. D'δ is derived from the measured concentration-penetration data by the use of [Eq. 2]. The value of the lattice diffusivity is taken from D = 1.1 exp(96,000/RT), (Ref. 7), δ is taken to be $5x10^{-8}$ cm, $\beta = D'/D \dfrac{1/2\delta}{(Dt)^{1/2}}$.

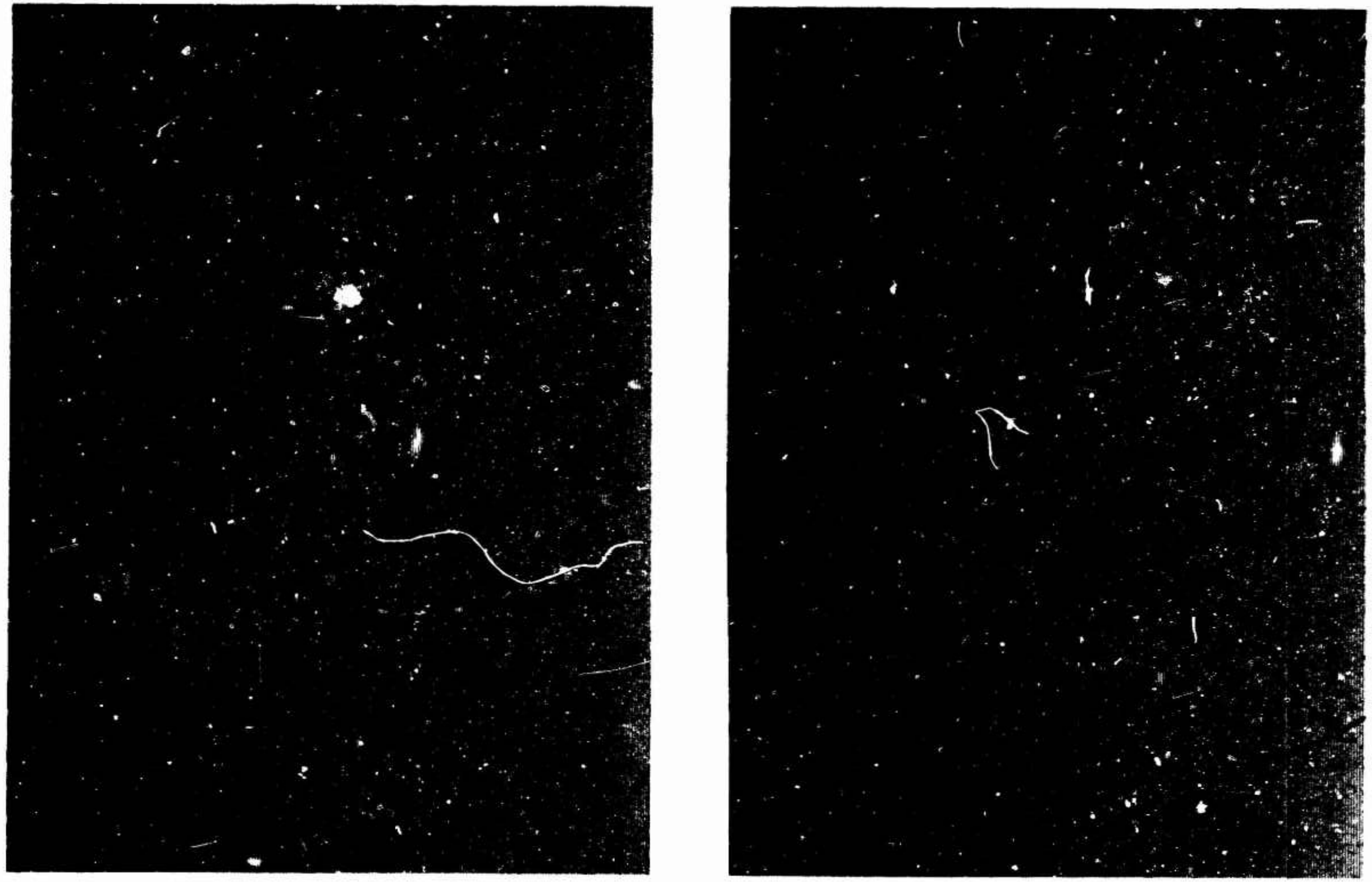

Fig. 3-1 - $\{111\}$ surface, electroetched 1 min. at 0.25 volt. 200X. (a) as grown (b) same area, light carbon deposit annealed 16 hr. at 1050°C

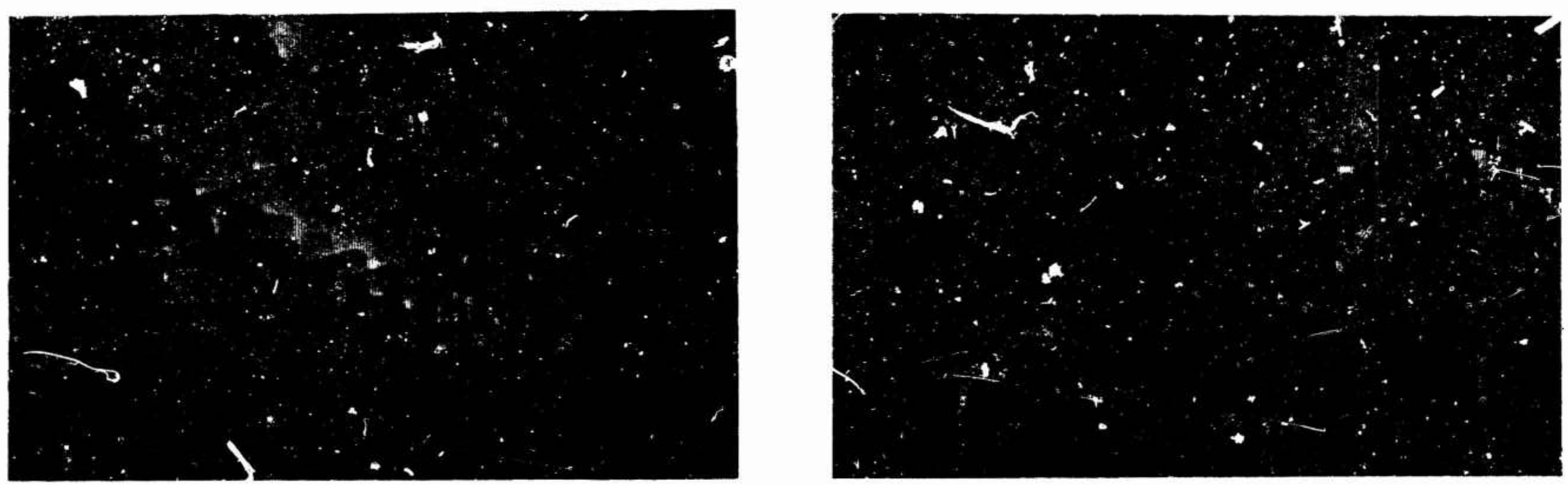

Fig. 3.2 - {111} surface, heavy carbon deposit annealed 16 hr. at 1050°C, etched $HNO_3 + HF$. 1035X, oblique light. (a) and (b) are successive stages of etching.

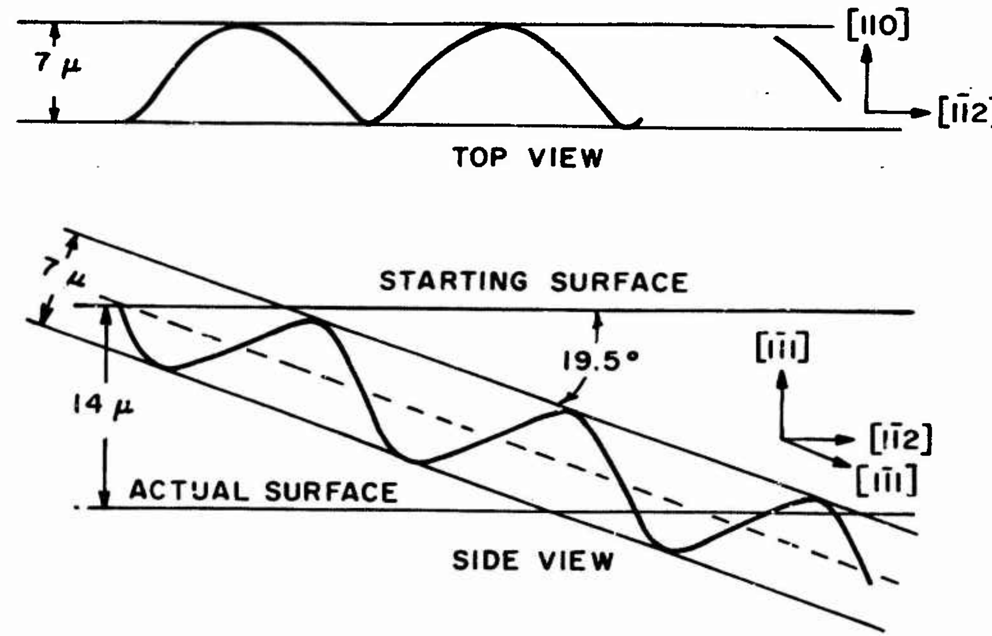

Fig. 3-3 - Top and side views of one half the double helix of 4(a) showing orientation and layer thickness

Fig. 3-4 - {111} surface, heavily doped, chemically etched, then electroetched. 485X, oblique light.

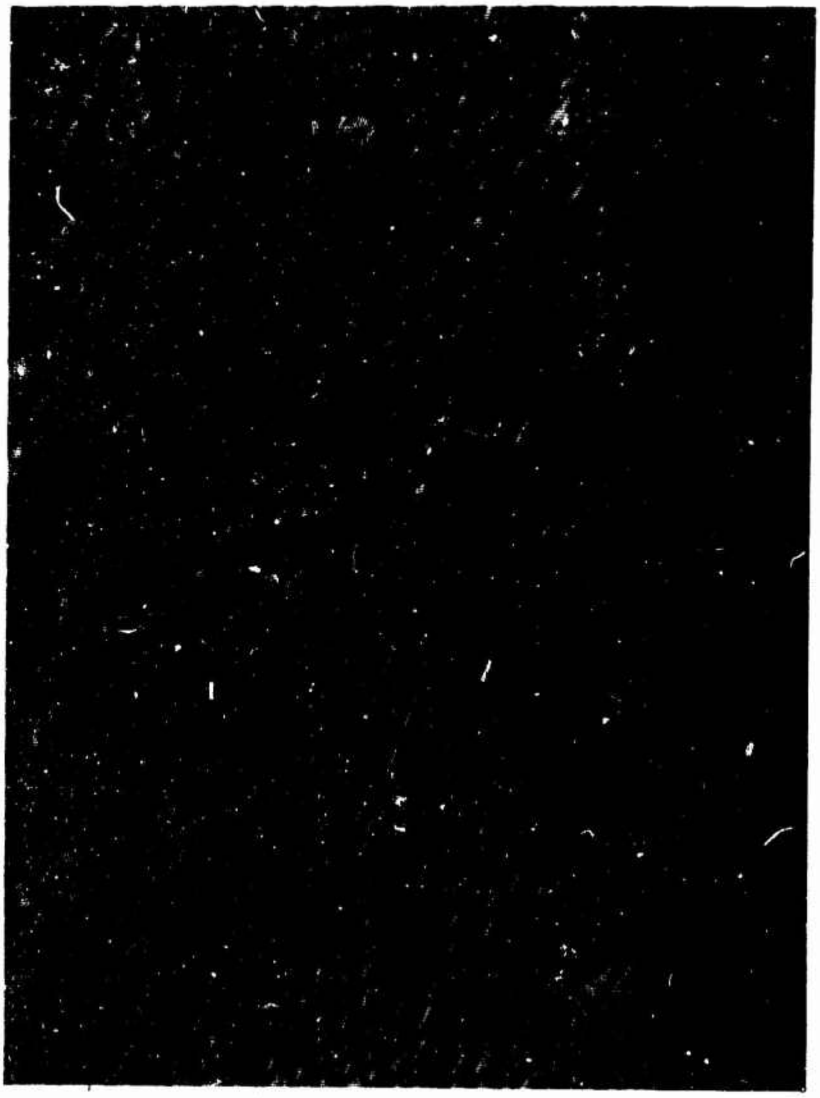

Fig. 3-5 - $\{110\}$ surface, heavily doped, chemically etched, 1750X, oblique light

Fig. 3-6 - {111} surface, heavily doped, chemically etched, 950X, oblique light

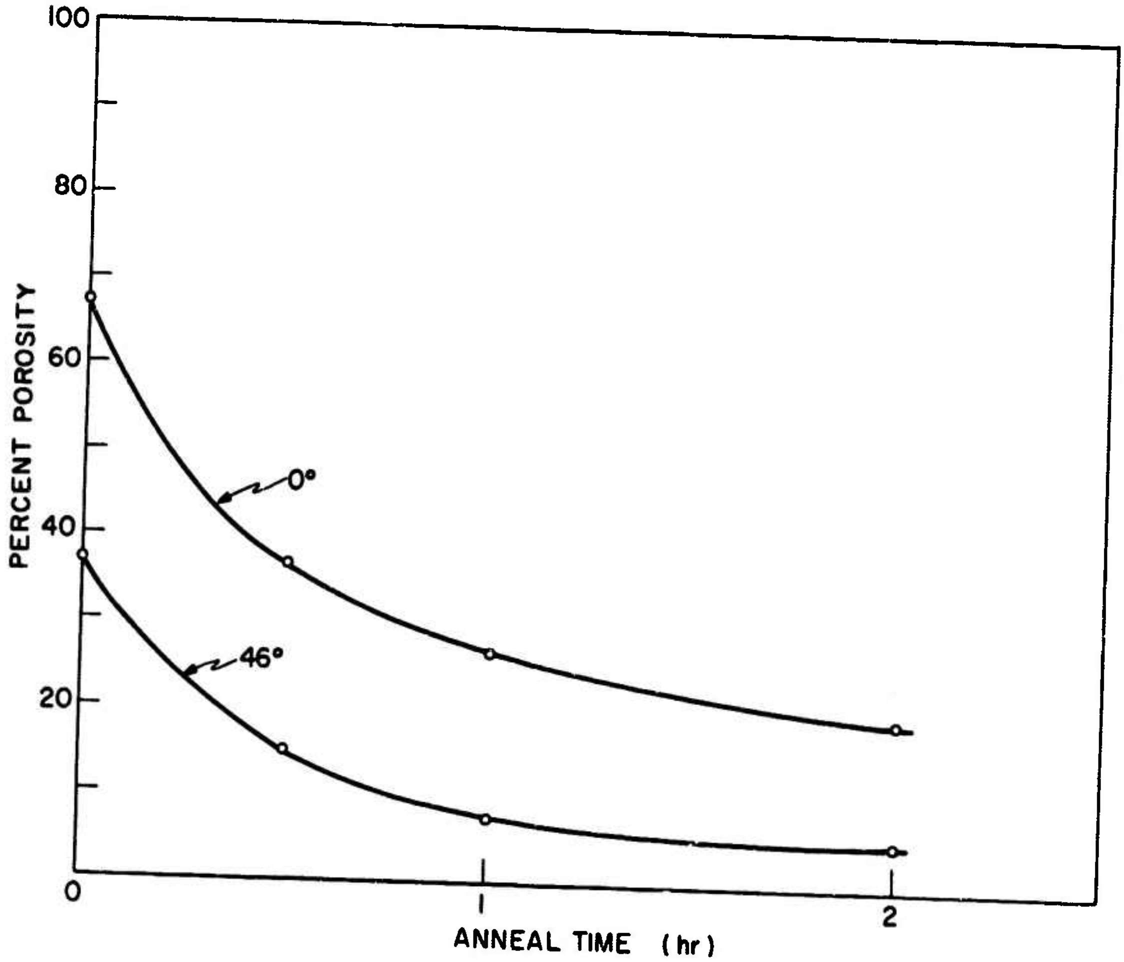

Fig. 4.1 - Annealing curves for 0° and 46° tilt boundary bicrystals, welded 5 min. at 300 psi and 1500°C

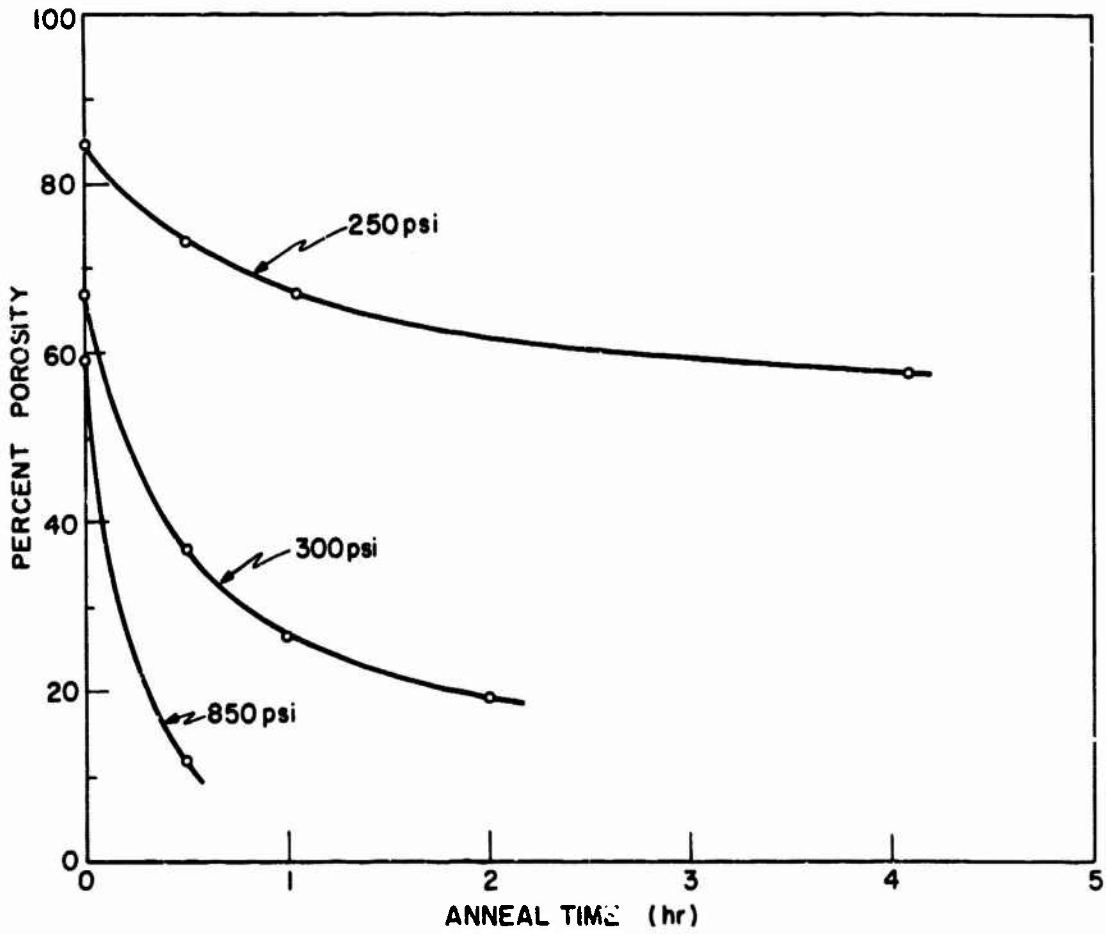

Fig. 4.2 - Annealing curves for 0° bicrystals welded at indicated pressures

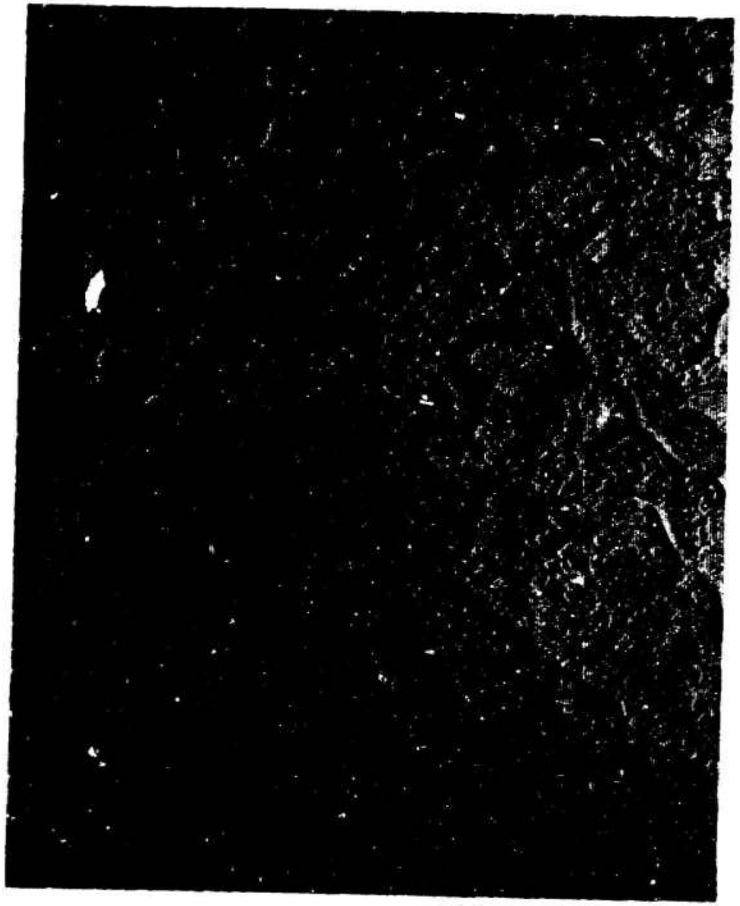

Fig. 4-3 - Bicrystal welded 5 min. at 300 psi, surface near {211}, heavily doped and chemically etched. 300X, oblique light. (a) as welded (b) annealed 1 hr. at 1800°C.

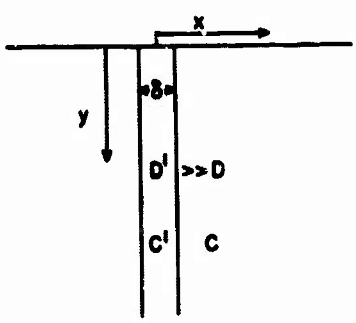

Fig. 5.1 - The model for grain boundary diffusion (1).

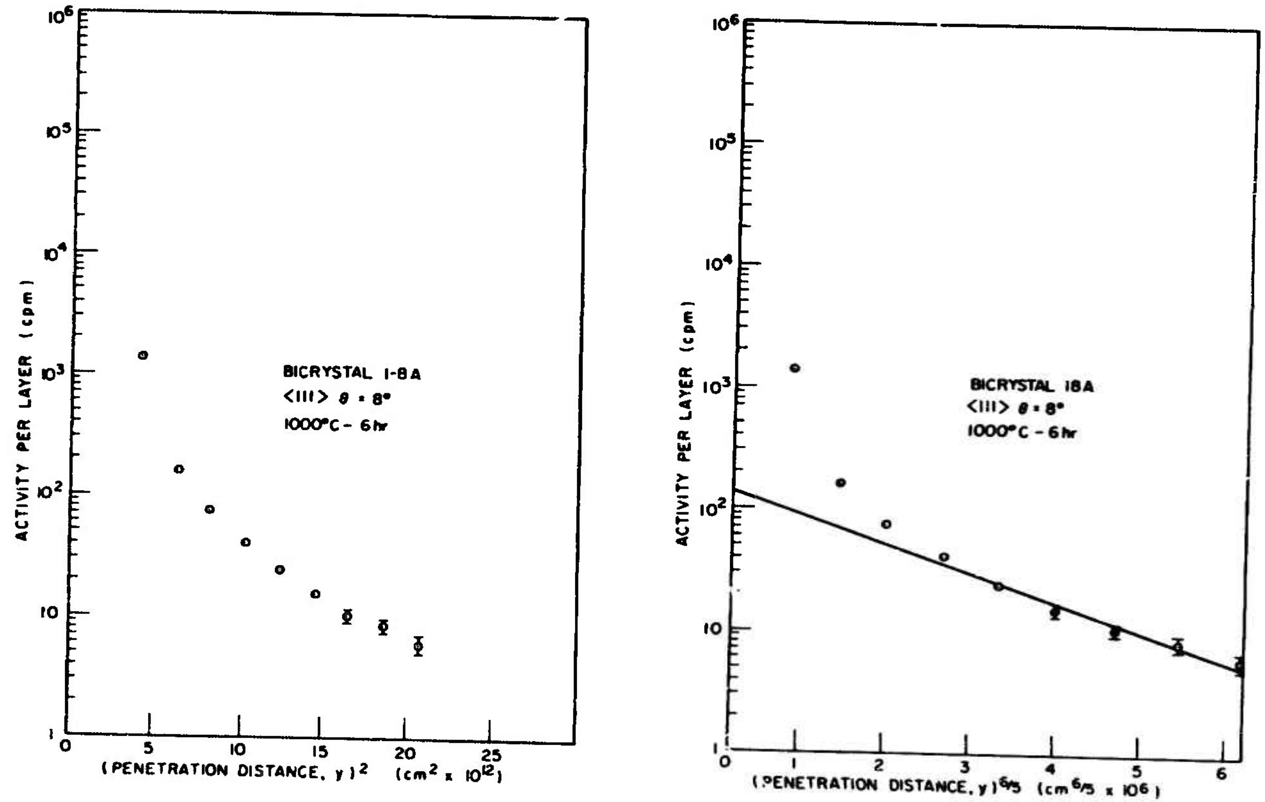

Fig. 5-2 - Concentration-penetration curves for grain boundary self diffusion in symetrically tilted 8° about <111>. Diffused 6 hr. at 1000°C.

Security Classification

DOCUMENT CONTROL DATA - R & D

(Security classification of title, body of abstract and indexing annotation must be entered when the overall report is classified)

1. ORIGINATING ACTIVITY (Corporate author) Naval Research Laboratory Washington, D.C. 20390	2a. REPORT SECURITY CLASSIFICATION Unclassified 2b. GROUP

3. REPORT TITLE

PREPARATION AND CHARACTERIZATION OF ULTRA-PURE SOLIDS -- ANNUAL REPORT JULY 1, 1966 -- JUNE 30, 1967 ON ARPA ORDER 418

4. DESCRIPTIVE NOTES (Type of report and inclusive dates)

An interim annual report July 1, 1966 - June 30, 1967

5. AUTHOR(S) (First name, middle initial, last name)

C.C. Klick, G.T. Rado, M.R. Achter, and A.I. Schindler

6. REPORT DATE	7a. TOTAL NO. OF PAGES	7b. NO. OF REFS
1967	79	36

8a. CONTRACT OR GRANT NO. NRL Problem Nos. M01-09, M01-10, P02-02, and P03-07 b. PROJECT NO. ARPA Order 418 c. d.	9a. ORIGINATOR'S REPORT NUMBER(S) NRL Memorandum Report 1815 9b. OTHER REPORT NO(S) (Any other numbers that may be assigned this report)

10. DISTRIBUTION STATEMENT

This document has been approved for public release and sale; its distribution is unlimited.

11. SUPPLEMENTARY NOTES	12. SPONSORING MILITARY ACTIVITY ARPA

13. ABSTRACT

The Naval Research Laboratory is conducting a broad investigation on the preparation and characteristics of ultrapure imperfection-free solids in an effort to improve our understanding of the relationships between the behavior of materials and their fundamental physicochemical make-up.

Specific efforts during 1966-1967, as was the case in previous annual reports for 1964-1965 and 1965-1966, included a wide range of theoretical and experimental studies on crystal growth kinetics, metallic behavior, the nature of interactions responsible for the magnetic properties of spin-ordered materials, and optical and radiation-sensitive properties of non-metallic materials. The properties investigated were correspondingly wide, as were the types of materials chosen for study which included refractory and transition metals and alloys, intermetallic compounds, alkali halides, glasses, and certain spin-ordered substances.

Four areas of investigation showing considerable progress during the year starting July 1966 are discussed herein. These investigations, each under the cognizance of a separate research group at the Laboratory, cover accomplishments on glasses and alkali halide crystals, refractory metal crystals, transition metal crystals, and magnetic materials.

During the first portion of the past year the program on preparation of ultrapure alkali halide crystals continued the further development of methods of purification of raw materials, methods of crystal growth, and characterization of the final products. Several projects within the Optical Materials Branch were appreciably aided

continued page 76

S/N 0101-807-6801

Security Classification

14. KEY WORDS	LINK A ROLE	LINK A WT	LINK B ROLE	LINK B WT	LINK C ROLE	LINK C WT
Solids						
Alkali halides						
Magnetic materials						
Refractory metal crystals						
Transition metal crystals						
Intermetallic compound single crystals						
Ultra-pure solids						
Single crystals						
Electron spin resonance						

by the resources developed in this program. Several months after the beginning of the report year a proposal was made to enlarge in a very substantial way the effort going on in glasses and to emphasize the research aspects concerned with understanding the most fundamental properties of glass. Approval of the plan came near the beginning of the present calendar year. The character of the work changed dramatically during the last portion of the year from concentration on alkali halides to major effort on glasses. Three new members were added to the staff of the Optical Materials Branch in anticipation of the acceptance of the program and numerous other members of the staff began to work intensively in the field of glass science. The result has been an active and closely coordinated group involving materials preparation, experiment, and theory. Detailed results obtained in the alkali halide and glass programs are discussed.

The long term objective of the program on refractory metals was the preparation and study of highly perfect specimens in which the only structural feature was a grain boundary of controlled misorientation. To achieve this purpose it was necessary to develop techniques for the production of highly perfect single crystals and for joining them to make bicrystals of controlled-misorientation. Program accomplishments have been made in five areas: (a) growth of single crystals of niobium; (b) characterization of single crystals by X-ray techniques; (c) optical observation of dislocation structures; (d) sintering of intergranular porosity; and (e) grain boundary self-diffusion in bicrystals.

Major progress in the program on transition metal and intermetallic compound single crystals included: (a) development of methods for applying high-resolution electron microscopy to the study of metallic crystal growth; (b) development of mathematical procedures for theoretical analysis of time-dependent crystal growth during embryonic stages of growth in both supercooled and hypercooled melts; (c) the first kinetic measurements of crystal growth in a hypercooled melt, which lead to a unique analysis of dendritic growth at extreme levels of supercooling; (d) establishment of a new theoretical approach for determining atomic attachment mechanism for crystal growth in metals, semiconductors and congruently-melting inter-metallic compounds; (e) measurement of the thermal conductivity of high-purity rhenium and palladium from 2-20°K and showing the existence of a new electron-electron collision term for the thermal conductivity of these metals; (f) the first experimental verification of the presence of electron-paramagnon scattering in high-purity palladium; and (g) the determination to high precision of the neck-orbit dimensions for the Fermi surface of high-purity copper via magnetoacoustic techniques.

In the program on the crystal synthesis and characterization of magnetic materials, progress in the synthesis area included construction of a vacuum single crystal furnace for avoidance of oxidation during crystal growth, partial construction of apparatus which will permit pretreatment of fluoride starting materials in HF to eliminate hydrate oxide and basic salt impurities, and the preparation of a series of α Al_2O_3 single crystals doped with Fe^{3+} at different concentration levels. Progress in the area of characterization included: (a) optical absorption studies of K_2CoF_4; (b) ESR studies of single crystals of K_2ZnF_4 doped with Mn^{2+} and single crystals of K_2ZnF_4 doped with Fe^{3+}; and (c) optical and ESR studies of single crystals of α-Al_2O_3 doped with Fe^{3+}.